AD-A266 238

WL-TR-93-3018

VALIDATION OF THE WL/FIM TRISONIC
GASDYNAMIC FACILITY FOR EXHAUST NOZZLE
TESTING

ROBERT D. GILLGRIST

FLIGHT DYNAMICS DIRECTORATE
WRIGHT LABORATORY
AIR FORCE SYSTEMS COMMAND
WRIGHT PATTERSON AFB OH   45433-7562

APR 92

FINAL REPORT FOR 01/01/90-03/31/92

APPROVED FOR PUBLIC RELEASE; DISTRIBUTION IS UNLIMITED.

93 6 28 001

93-14683

FLIGHT DYNAMICS DIRECTORATE
WRIGHT LABORATORY
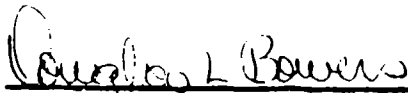AIR FORCE MATERIEL COMMAND
WRIGHT-PATTERSON AIR FORCE BASE, OHIO 45433-7562

NOTICE

This technical report has been reviewed and is approved for publication.

DOUGLAS L. BOWERS
Aerospace Engineer
Aerodynamics & Aero Components
Research Branch

LEWIS E. SURBER
Tech Manager
Aerodynamics & Aero Components
Research Branch

DAVID R. SELEGAN
Chief
Aeromechanics Division

REPORT DOCUMENTATION PAGE

Public reporting burden for this collection of information is estimated to average 1 hour per response, including the time for reviewing instructions, searching existing data sources, gathering and maintaining the data needed, and completing and reviewing the collection of information. Send comments regarding this burden estimate or any other aspect of this collection of information, including suggestions for reducing this burden, to Washington Headquarters Services, Directorate for Information Operations and Reports, 1215 Jefferson Davis Highway, Suite 1204, Arlington, VA 22202-4302, and to the Office of Management and Budget, Paperwork Reduction Project (0704-0188), Washington, DC 20503

1. AGENCY USE ONLY (Leave blank)	2. REPORT DATE	3. REPORT TYPE AND DATES COVERED
	Apr 92	FINAL 01/01/90 - 03/31/92

4. TITLE AND SUBTITLE Validation of the WL/FIM Trisonic Gasdynamics Facility for Exhaust Nozzle Testing	5. FUNDING NUMBERS
	C
	PE 62201
	PR 2404
6. AUTHOR(S) Robert D. Gillgrist	TA 10
	WU B4

7. PERFORMING ORGANIZATION NAME(S) AND ADDRESS(ES)	8. PERFORMING ORGANIZATION REPORT NUMBER
Flight Dynamics Directorate Wright Laboratory Air Force Systems Command Wright Patterson AFB OH 45433-7562	WL-TR-93-3018

9. SPONSORING/MONITORING AGENCY NAME(S) AND ADDRESS(ES)	10. SPONSORING/MONITORING AGENCY REPORT NUMBER
Flight Dynamics Directorate Wright Laboratory Air Force Systems Command Wright Patterson AFB OH 45433-7562	WL-TR-93-3018

11. SUPPLEMENTARY NOTES

12a. DISTRIBUTION/AVAILABILITY STATEMENT	12b. DISTRIBUTION CODE
Approved for public release; distribution is unlimited	

13. ABSTRACT (Maximum 200 words)

The Wright Laboratory's expanding requirement for reliable resident exhaust nozzle testing capability necessitated the verification of the experimental capability of the Trisonic Gasdynamics Facility (TGF) located at Wright-Patterson Air Force Base. A validation test, directed toward the TGF's nozzle testing capability, compared surface pressure data taken from an axisymmetric AGARD reference nozzle from a wind tunnel test performed at the Propulsion Wind Tunnel (PWT) at Arnold Engineering Development Center (AEDC). Boattail pressure distributions and pressure drag measurements were compared between the facilities. Cross-sectional blockage caused significant differences between boattail pressures and pressure drag coefficients between facilities. Computational fluid dynamics (CFD) tools were used to aid understanding of differences found in the comparison study. A series of CFD simulations aimed at determining the actual freestream flow Mach number is recommended to improve flow simulating accuracy in the TGF.

14. SUBJECT TERMS			15. NUMBER OF PAGES
Wind Tunnel, Simulation, Drag, Validation, Boattail, Computational Fluid Dynamics (CFD), Pressure Coefficient. Blockage			86
			16. PRICE CODE

17. SECURITY CLASSIFICATION OF REPORT	18. SECURITY CLASSIFICATION OF THIS PAGE	19. SECURITY CLASSIFICATION OF ABSTRACT	20. LIMITATION OF ABSTRACT
Unclassified	Unclassified	Unclassified	UL

NSN 7540-01-280-5500

DTIC QUALITY INSPECTED 1

PREFACE

TABLE OF CONTENTS

LIST OF ILLUSTRATIONS

LIST OF SYMBOLS

C_p	Pressure Coefficient
C_D	Drag Coefficient
C_{DTP}	Pressure-Area Integrated Drag Coefficient
NPR	Nozzle Pressure Ratio
PN(i)	Internal Rake Total Pressure
P_S	Freestream Static Pressure
P(K)	Surface Pressure
D	Maximum Body Diameter
A_{ref}	Reference Area For C_{DTP} Calculation
M	Mach Number
Q	Dynamic Pressure
g	Specific Heat Ratio

INTRODUCTION

There is a continuing need for a reliable, subscale wind tunnel testing capability for nozzle boattail and afterbody configurations in Wright Laboratory's Aeromechanics Division (WL/FIM). The Aeromechanics Division's 2-foot Trisonic Gasdynamics Facility (TGF) has been used by engineers in WL/FIM to screen innovative advanced exhaust nozzle concepts prior to potential full-scale testing. In recent TGF exhaust nozzle tests, questions have been raised regarding the accuracy of surface pressure data, the repeatability of experimental data, and the correctability of these data. The hypothesis is that excessive tunnel blockage, where blockage is defined as the ratio of model and support hardware cross-sectional area to test section cross-sectional area, results in inaccurate freestream tunnel flow.

To establish the validity of exhaust nozzle testing in the TGF, a comparative study was performed on two similar databases of nozzle boattail pressures. The first database was taken from a TGF test on 10- and 15-degree AGARD axisymmetric boattails. The second database is taken from a similar test of axisymmetric AGARD nozzles from a reliable industry accepted facility, Arnold Engineering Development Center's (AEDC) Propulsion Wind Tunnel 16-foot transonic facility (PWT 16T). Specifically, model surface pressures from the test conducted in the TGF in early 1989 were

compared to pressures from a similar nozzle test conducted in the 16T in 1975. Computational Fluid Dynamics (CFD) tools were used to help us understand the data comparisons. The following report discusses details of the TGF experiment, the comparison of the TGF and 16T data, and the CFD techniques employed. Implications of these analyses are then summarized, and recommendations are made for future nozzle testing in the TGF.

TECHNICAL DISCUSSION

Wind Tunnel Description

The Trisonic Gasdynamics Facility (TGF) is a closed circuit, continuous flow, variable density wind tunnel capable of operating at subsonic, transonic, and supersonic Mach numbers. A subsonic test section allows operation from Mach 0.23 to Mach 0.85. A supersonic test section uses four fixed area ratio nozzles to test at Mach 1.5, 1.9, 2.3, and 3.0. The subsonic and supersonic test sections are 24 in. X 24 in. square. A schematic of the tunnel is shown in Figure 1 *. The TGF User's Manual contains additional tunnel information1.

The AEDC PWT 16T is a continuous flow, variable density, closed circuit wind tunnel which operates at Mach numbers from 0.2 to 1.6. The test section is 16 ft X 16 ft square. The test facilities handbook for the PWT may be consulted for additional information2.

Test Hardware Description

The experiment conducted at the TGF in January and February of 1989 acquired pressure data from a nozzle connected to a simple axisymmetric forebody. General

* **Figures 1 thru 33 begin on page 26**

Dynamics/Fort Worth designed the convergent nozzle test body shown attached to a sting and short forebody mount in Figure 2a. Model components were fabricated by Wright Laboratory. Both a 10- and a 15-degree AGARD reference boattail configurations were tested. The reference boattail angle is defined as the angle made by a line connecting the leading and trailing edges of the boattail contour with the horizontal. (See Figure 2b.) A cylindrical forebody insert (not shown in Figure 2) was removed for supersonic test runs to prevent interactions between the boattail and shock reflections from the tunnel walls. The test body also had two nose pieces: a rounded nose for subsonic testing and a sharp nose piece for supersonic testing.

The test hardware was fabricated to meet certain system design requirements and to be compatible with the existing support hardware in the TGF. Figure 3 depicts the TGF test body mounted in the tunnel on its strut and sting assembly which extends from an access panel located downstream of the test window. The strut houses wiring for model instrumentation and contains a high pressure air line to provide sufficient flow for representative exhaust expansion. Internal thrust sleeves of both the 10- and 15-degree configurations were also designed and fabricated to isolate the external boattail flow and the internal jet flow. Each sleeve was designed to fit within each nozzle configuration with a minimum gap at the trailing edge. Eighty-one external static pressure taps were systematically

4

placed about the nozzle circumference and along its length (Figure 4). Internal pressures were measured by four static and five total pressures. A single component, flow through ring balance was calibrated to measure forces applied to the exterior shell. The force balance data from the TGF test, however, was not used in the facility comparison since no force balance data were taken during the AEDC 16T test.

The 16T test also used the AGARD reference boattails connected to a longer forebody. Figure 5 shows a schematic of the 16T model mounted to a simple vertical strut. Figure 6 presents dimensioned drawings of both models. Note that the 16T and TGF forebodies are not scaled relative to each other. When the 16T test body was scaled to 31.95% of its full model dimensions, the most accurate geometric boattail pressure data comparisons were made.

The 16T test forebody was instrumented with 24 forebody pressure taps, a forebody boundary layer rake, a pressure rake mounted in the cold flow duct, and four internal static pressure taps. The 10- and 15-degree boattail configurations had 82 and 75 surface pressure taps, respectively. A dimensioned schematic of the 16T model arrangement is shown in Figure 73.

Figure 8 summarizes the relevant tunnel and model dimensions for both experiments. Note that the cross-sectional blockage in the TGF test was 1.352%, approximately 6.5 times more than the blockage in the 16T test.

Typically, an industry "rule of thumb" is a 1.0% blockage or higher is considered undesirable for exhaust nozzle testing.

Testing

The matrix of flow parameters used in the test is shown in Figure 9. Both the 10- and 15-degree boattails were tested at several Nozzle Pressure Ratios (NPRs) for each test condition listed. Data were acquired for 505 test runs total. Testing on this project in the TGF was completed by February 1989.

Equations used to reduce the surface pressure data are listed in Appendix A. Boattail pressure distribution plots comparing 16T test results with the TGF test data were produced at the conclusion of the test. Figure 10 shows one example of these plots.

Data Comparisons

Comparisons to validate the afterbody testing capability of the TGF were established between the 16T database and the TGF database. Appendix B shows which data runs were compared. Only data runs that shared the same Mach number, NPR, and boattail angle were compared. Only conditions at Mach 0.6 and Mach 0.8 could be directly studied.

Comparisons were made between pressure coefficients (CP's) and pressure-area integrated drag coefficients (CDTP's) between the two facilities. Appendix A contains the equations that define CP and CDTP for this comparison. CDTP is the pressure-area integrated drag coefficient using the top row of pressure orifices, assuming a uniform surface pressure distribution around the test body circumference. The strong influence of the model support strut in the flowfield necessitate using the unaffected top row of pressures.

AEDC 16T and TGF pressure coefficients and pressure drag coefficients were compared using two different methods. One comparison was of absolute values of 16T data versus TGF data and comparison of the respective magnitudes at appropriate forebody and boattail stations. This quantitative comparison aided the understanding of how well the two test articles matched each other under specified conditions. The small model in the large AEDC tunnel suggests using the AEDC data as a reference for the TGF data. Taking the AEDC data as correct, this comparison method also aided in understanding of how accurately the TGF and its test article were able to simulate the specified conditions. A second scheme compared how data from each tunnel responded to changes in flow and test parameters (such as tunnel Mach number, NPR, or boattail angle). Two plots are used to make this kind of sensitivity comparison. A first plot shows several sets of data from one tunnel for

discrete values of a single flow parameter. The second plot
shows the same data set for the second tunnel. The
differences in the data as a parameter is changed were
compared for the tunnels. For example, a qualitative
incremental comparison may be made showing how different
values of NPR affect the upper centerline pressure
distribution for a specific Mach number and nozzle in each
tunnel. By using both comparison techniques, a greater
understanding of tunnel differences in the data was
obtained. For the purposes of the following discussion, the
first comparison method shall be denoted as the absolute
method and the second as the incremental method.

Results of Comparison

Absolute comparisons between pressure coefficients at
eight Mach number/boattail angle conditions are shown in
Figures 11 (a-h). TGF pressures are significantly different
in magnitude than the corresponding 16T pressures at each
condition shown. Note that the difference between pressure
distribution magnitudes is greater at the four Mach 0.8
cases shown here (Figures 11(c), 11(d), 11(g) and 11(h))
than at the Mach 0.6 cases (Figures 11(a), 11(b), 11(e), and
11(f)).

This consistent discrepancy between surface pressure
coefficients is presumed to be attributable to cross-
sectional blockage in the TGF tunnel. A simple application

8

of the one-dimensional continuity and Bernoulli equations suggests that in regions of high blockage the freestream flow accelerates, increasing the local Mach number and causing significant static pressure reduction.

Data from a 1984 TGF test on a circular arc axisymmetric nozzle indicated the effects of a similar blockage problem. Figure 12, taken from the 1984 test report (Reference 4), shows a pressure reduction across the straight forebody section (stations 206-224) of the model. This pressure reduction, occurring where near freestream conditions are typically expected, appears similar to forebody pressure reductions seen previously in Figures 11 (a-h). This supporting evidence strengthens the assertion that excessive tunnel blockage causes the flow discrepancies seen in the previous figures.

Figures 13 (a-d) show incremental comparisons of pressure distribution at four NPRs between the two facilities. Figures 13(a) and 13(b) compare Mach 0.6 data between facilities, and Figures 13(c) and 13(d) compare Mach 0.8 data between facilities. At first glance these distributions appear relatively insensitive to pressure ratio. A closer investigation, however, shows that lower NPRs yield slightly lower pressure coefficients across the nozzle for the 16T data. The 16T jet-off conditions yield lower pressure readings than corresponding jet-on distributions, while TGF jet-off conditions do not depart as drastically from jet-on distributions. Differences between

9

16T Cp distributions appear uniform across the boattail, while the differences between TGF distributions are inconsistent.

Comparisons of 10- and 15-degree aftbody boattail pressure distributions at similar flow conditions are presented in Figures 14 (a,b) for each model in its respective facility. The 16T data show a larger and more uniform difference between distributions. Differences in TGF data vary widely over the boattail.

Drag coefficient measurements were also used to make absolute comparisons of the two test databases. Figures 15 (a,b) show CDTP plotted against Mach Number at NPRs of 2.0 and 4.0. The TGF data show substantially higher pressure drag coefficients than encountered in 16T data. TGF data also shows a drag rise with increasing Mach number which is not seen in 16T data. A typical CD vs. Mach number plot for a generic nozzle boattail (Figure 16) shows the same drag rise occurring with increasing Mach number, but at Mach numbers greater than 0.85. This further supports the thesis that blockage effects in the TGF test section increased the actual flow Mach number around the model.

Comparisons between CDTP vs. Mach Number at several NPRs were also made between facilities. Figures 17 (a,b) show such comparisons for the 10-degree boattail. Both figures show high NPRs yielding the lowest boattail drag measurements, an expected result. Note also that jet-off

conditions yield significantly higher drag measurements than all jet-on conditions in both plots.

Drag coefficients are plotted against NPR in Figures 18 (a,b). The shape of the curves shown are typical of a typical CD vs. NPR graph, as shown in Figure 195. TGF drag values are still noticeably higher than their 16T counterparts, especially at the highest Mach number. Once again, this offers additional support of the hypothesis that excessive tunnel blockage affects measuring of experimental flow parameters.

CFD VERIFICATION STUDY

CFD Simulation Description

To verify the conclusion that tunnel blockage is the primary cause of observed data discrepancies, a verification study of each wind tunnel test was performed using CFD. The approach was to simulate both experiments by modelling both wind tunnel test sections and placing each test body with its respective support structure into the proper flowfield. Three-dimensional grid generation techniques were then used to build a computational domain for each test section. An algorithm that solved the inviscid equations of motion was then employed to numerically generate flowfield data. The computational data were compared with the experimental pressure distributions with the goal of verifying the effects of blockage on experimental pressure and drag measurements.

Several computer codes were used to generate the structured grid geometry. The I3G/VIRGO, an interactive, graphical geometry database editor, was used to create a three-dimensional surface database of each tunnel[6]. The GRIDGEN series of codes, GRIDBLOCK and GRIDGEN2D, was used to divide the domain into zones and generated structured 2D meshes for each block face[7]. PLUTO3D, an inhouse code, was

used to create the three-dimensional meshes interior to each block. The I3G/VIRGO, GRIDBLOCK, and GRIDGEN2D are all interactive codes and were run on Silicon Graphics IRIS Workstations. PLUTO3D was run in a batch processing mode on a CRAY X-MP supercomputer.

These three-dimensional structured grids were numerically evaluated using the MERCURY flow solver[8]. The MERCURY code solves Euler's equations of motion for three-dimensional, multiblock grids. The flow-solving algorithm is based on Jameson's finite volume, cell-centered, four-stage Runge-Kutta method with blended second and fourth order artificial damping[9]. MERCURY was run on a CRAY X-MP 216. Inhouse plotting packages were used to compare experimental and CFD data. PLOT3D, a graphical, interactive postprocessing package, was used to view the 3D flow solution in selected blocks for diagnostic purposes (Reference 12.)

Results of CFD Simulation

Figures 20 (a,b) show the block structures used to grid the AEDC 16T and TGF test sections, respectively. Both block structures model the flowfields around the 10-degree boattail configurations. Due to symmetrical flow conditions, only half of the test section was gridded. The blocking strategy used three rows of blocks top to bottom to divide the flowfield around the test article. This allows

13

tight mesh spacing near the strut and sting without passing such spacing onto other faces radially about the test section centerline. The streamwise block structure places block interfaces far from regions of high gradients. This also minimizes the number of boundary conditions on each face normal to the stream. An aft-facing step located behind the sting mount in Figure 20(b) was altered considerably to acceleratre convergence.

Figures 21 (a-d) show two- and three-dimensional pictures of the 16T and TGF flowfield grids, respectively (for presentational purposes, not every grid line is shown in these figures). The 16T grid contained 11 blocks and 620,303 grid points while the TGF grid contained 20 blocks and 934,419 grid points. Uniformity of spacing between adjacent blocks was enforced, especially near the surface of the model. Dense spacing was employed at the highly rounded nose and boattail regions of the model.

Four flow conditions were studied for each test section, i.e. AEDC 16T and TGF. Figure 22 shows the matrix of flow conditions analyzed using CFD. Convergence criteria used for the CFD solutions were (1) C_p values measuring approximately 0.0, indicating forebody freestream flow, (2) an inviscid stagnation region fully formed at the model nose (C_p's approximately 1.0), and (3) a fully established boattail flow.

Using only the upper centerline Cp data, Figure 24 shows how computed pressure coefficients compare to AEDC 16T

14

experimental data for teh same flow parameters.
Experimental pressures along the body of the test article
compare well with the Euler results while pressures measured
in the boattail region do not. Euler solutions do not
capture the viscous phenomena occurring on the nozzle
boattail as shown at higher NPRs, Figure 25. Figures 26 and
27 show the same two nozzle pressure settings at a
freestream Mach number of 0.8. In all four cases shown,
inviscid solutions predict the upper forebody centerline
pressures, but not the boattail pressures, on the 16T model
with reasonable accuracy.

Figure 29 shows numerically generated C_p contours on
the upper centerline of the TGF model at Mach 0.6 and NPR
1.04 compared tc experimental data. The forebody pressure
coefficients should be 0.0 for no blockage; the data show a
clear reduction Cp on the body of the TGF model. The fact
that the CFD solution accurately predicts this blockage
effect in the TGF test section is a significant result.
Similar results for NPR=3.0 are evident, as shown in Figure
30. Figures 31 and 32 show CFD comparisons at Mach 0.8 and
two NPRs. Both predict the effects of blockage in the TGF
test section.

Figure 33 shows the effect of blockage on the CFD
results from both test sections. Here a comparison is made
between two CFD solutions at the same flow parameters in
each tunnel. The CFD solutions show the same effects of
blockage as the experimental data. It was concluded that

15

Euler methods predict and confirm the effects of blockage in the TGF exhaust nozzle test.

CONCLUSIONS

The exhaust nozzle testing capability of the TGF was evaluated by comparing common surface pressure data from an industry standard facility, AEDC's PWT 16T. Comparisons of pressure data from similar AGARD boattail test entries in each tunnel show that blockage in the TGF's 2-square-foot test section causes a substantial surface pressure reduction along the body of the test article. A large, observed discrepancy in pressure-area integrated drag coefficient between the two facilities due to transonic drag rise is also caused by the accelerated flow around the test body.

To verify these conclusions and to establish a capability to numerically simulate wind tunnel flowfields and potentially correct for the blockage effects observed, inviscid CFD solutions of each tunnel flowfield were generated for a matrix of test conditions. Generally good agreement existed between the CFD solutions and the experimental data taken from each facility. The CFD confirms the effects of blockage encountered in the TGF test. These conclusions establish the adeqacy of Euler solvers to model subsonic exhaust nozzle wind tunnel flowfields.

RECOMMENDATIONS

Further comparisons between TGF surface pressure data
with pressure data from other low blockage, industry
standard wind tunnel facilities would serve to further
validate the conclusions made by this analysis. The
comparison of dynamic data collected from a force balance
would further confirm these conclusions. A database
prepared from a boundary layer displacement thickness study
for nozzle boattails from Lockheed-Georgia's Compressible
Flow Facility in Marietta, Georgia may be suitable for
further comparison studies[10].

One potential desired result of further comparisons may
be the establishment of correction factors that can be used
by tunnel operators to recalibrate tunnel Mach number
specifically for exhaust nozzle testing. Any such
correction factors would be a function of numerous
parameters, including tunnel Mach number, model cross-
sectional area, and tunnel static pressure. By using the
Design of Experiments approach, a 'significant' matrix of
test parameters that determine correction factor values
could be determined[11]. Further CFD testing could then be
used to determine the magnitude of the Mach number
correction factor for a given set of 'significant' test
parameters. The contents of this report will hopefully be a

first step in the optimization of the TGF's data-taking
accuracy for future exhaust nozzle integration concepts.

REFERENCES

1.   Clark, Capt. Gary F., "Trisonic Gasdynamic Facility User Manual," TM 73-82-FXM Revision 1, 1982.

2.   "Test Facilities Handbook, Propulsion Wind Tunnel Facility, Vol. 4," Arnold Engineering Development Center, Arnold Air Force Station, Tennessee, 1974.

3.   Galigher, L.L., Jackson, F.M. and Robinsc , C.E., "Description of the AGARD Nozzle Afterbody Experiments Conducted by AEDC. Tennessee," AGARDograph No. 208 on Improved Nozzle Testing Techniques in Transonic flow, 1974.

4.   Fujimura, Clay, "Conformal Nozzle Parametric Test: Entries One and Two," AFWAL-TM-87-192-FIMM, 1987.

5.   Rozendal, D., Grothoff, C.C., and Derksen, W.B., "Results of NLR Contribution To AGARD Ad Hoc Study," AGARDograph No. 208 on Improved Nozzle Testing Techniques in Transonic Flow, 1974.

6.   Emsley, H.T., "I3G/VIRGO, Interactive Graphics for Geometry Generation and Visual Interactive Rapid Grid Generation, User's Manual," WRDC-TM-90-317, Wright-Patterson AFB, OH, May 1990.

7.   Steinbrenner, J.P., Chawner, J.R., and Fouts, C.L., "The Gridgen 3D Multiple Block Grid Generation System, Volume II: User's Manual," WRDC-TR-90-3022, Fort Worth, TX, 1990.

8.   Strang, W.Z., "Mercury User's Manual," AFWAL-TM-88-217, Wright-Patterson AFB, OH, 1988.

9.   Jameson, A., et al., "Numerical Solutions of the Euler Equations by finite Volume Methods Using Runge-Kutta Time-Stepping Schemes," AIAA Paper 81-1259, June 1981.

10.   "AGARD NAB Study (Phase I) In the PWT (16T), Test Plan, TF 337," Arnold Engineering Development Center, Arnold Air Force Station, Tennessee, Feb. 1974.

11.   Ross, Phillip J., "Taguchi Techniques For Quality Engineering," McGraw-Hill, Inc., 1988.

12.   Walatka, Pamela P., "PLOT3D User's Mannual," NASA TM 101067, 1989.

Appendix A: Data Reduction Equations

PN(i) = Internal Rake Total Pressure

P_S = Free Stream Static Pressure

P(K) = Surface Pressure

D = Maximum Body Diameter

$A_{ref} = \dfrac{p}{4} D^2$

(1) Nozzle Pressure Ratio = NPR

$$NPR = \frac{\frac{1}{5} \, \mathring{a} \, PN(i)}{P_S}$$

(2) Pressure Coefficient = C_p

$$C_p = \frac{DP}{Q} = \frac{P(K) - P_S}{\frac{g}{2}(P_S) \, M^2}$$

(3) Afterbody Pressure Drag = C_{DTP}

$$C_{DTP} = \frac{p}{2A_{ref}} \, \mathring{a}_{i=x}^{n} \, (C_{pi} + C_{(pi+1)}) \, (R_i^2 - R_{(i+1)}^2)$$

Appendix B: Data Comparison Matrix (3 pages)

16T TPN	TGF TPN	Boattail Angle	Mach Number	NPR
6102	63 68 79	10	0.6	1.0
8603	63 68 79			
7002	63 68 79			
6106	65 78 86	10	0.6	2.0
8608	65 78 86			
7005	65 78 86			
6109	66 71 85	10	0.6	3.0
8609	66 71 85			
7008	66 71 85			
6113	67 74 84	10	0.6	4.0
6204	150 157 170	10	0.8	1.0
8702	150 157 170			
7102	150 157 170			

23

16T TPN	TGF TPN	Boattail Angle	Mach Number	NPR
7104	153 167 172	10	0.8	2.0
6211	155 161 173	10	0.8	3.0
8712	155 161 173			
7107	155 161 173			
6213	168 174 214	10	0.8	4.0
5601	189 202 214	15	0.6	1.0
4103	189 202 214			
1901	189 202 214			
1903	184 204 213	15	0.6	2.0
4107	184 204 213			
5604	184 204 213			
1913	185 205 212	15	0.6	3.0
5605	185 205 212			

16T TPN	TGF TPN	Boattail Angle	Mach Number	NPR
2004	215 221 230 246	15	0.8	1.0
4202	215 221 230 246			
4204	217 223 232 242	15	0.8	2.0
2014	217 223 232 242			
2019	218 224 237 243	15	0.8	3.0
4206	218 224 237 243			
2010	225 234 244	15	0.8	4.0
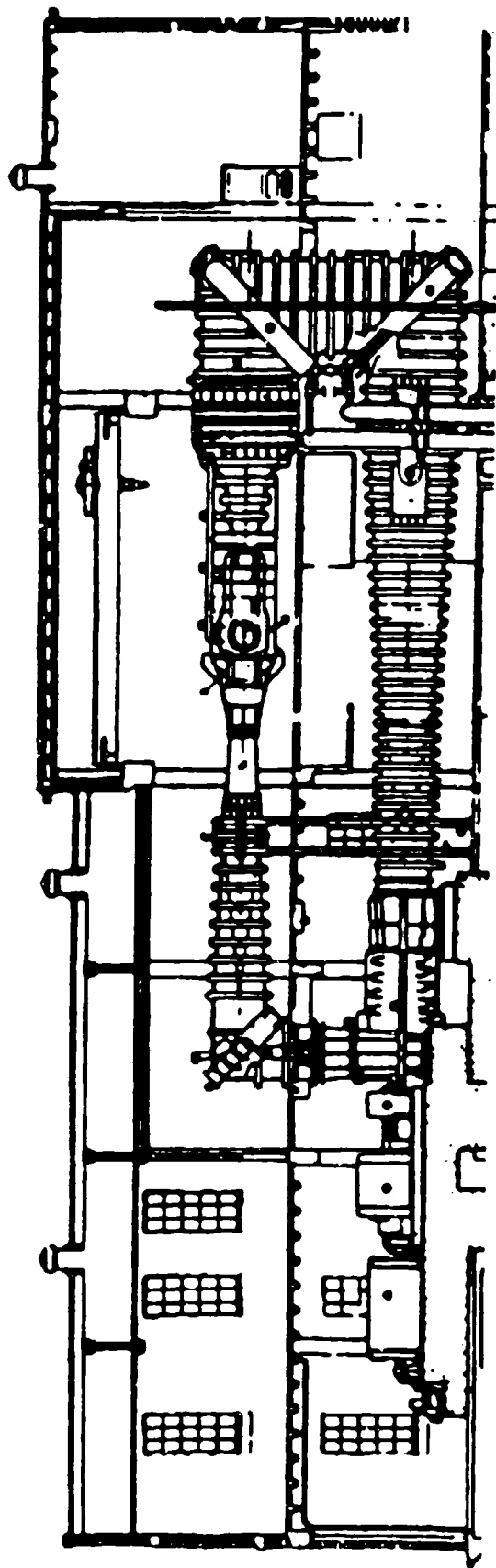
Figure 1. Trisonic Gasdynamics Facility (TGF) Schematic

26

Figure 4. Model and Support Hardware, FGF Test
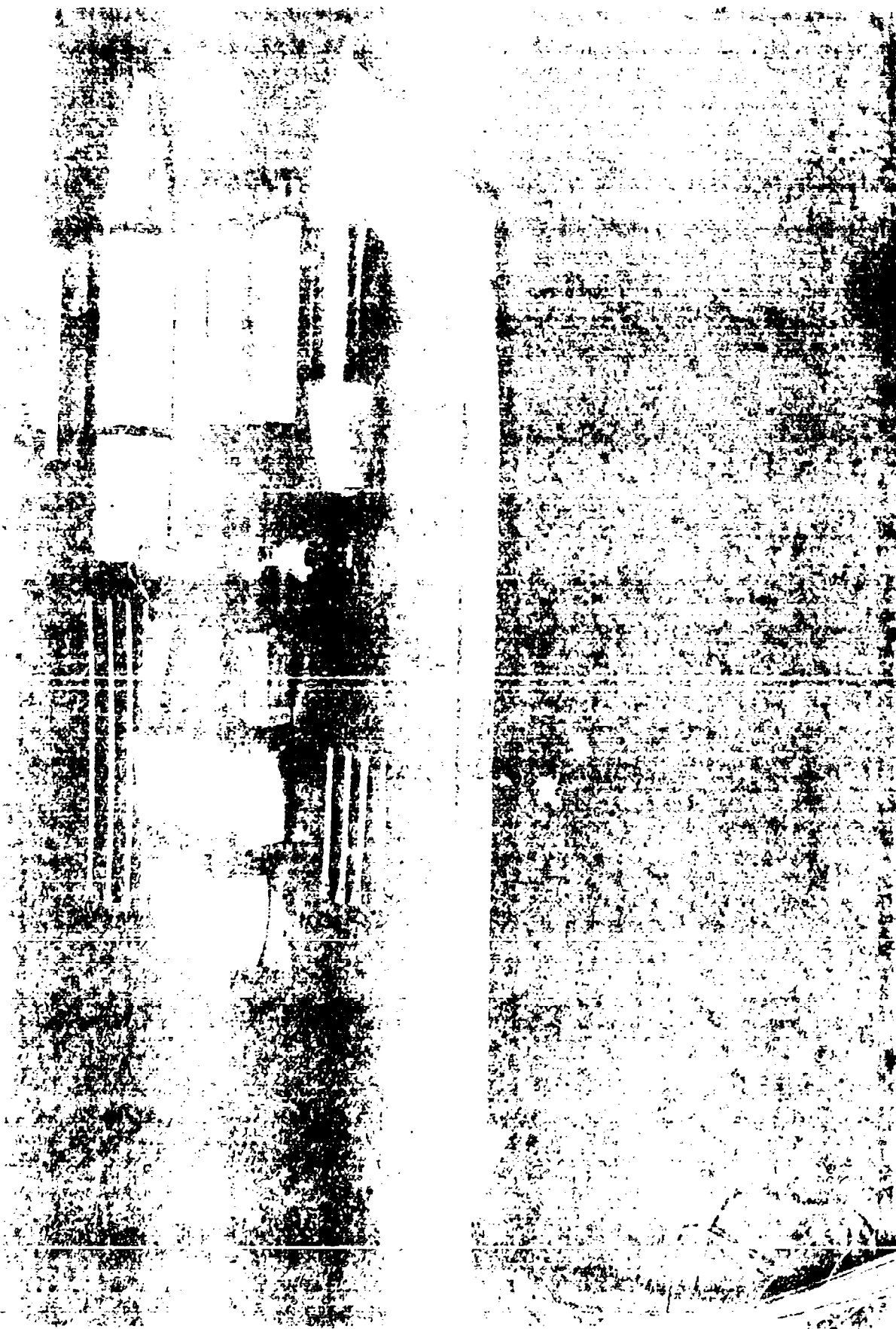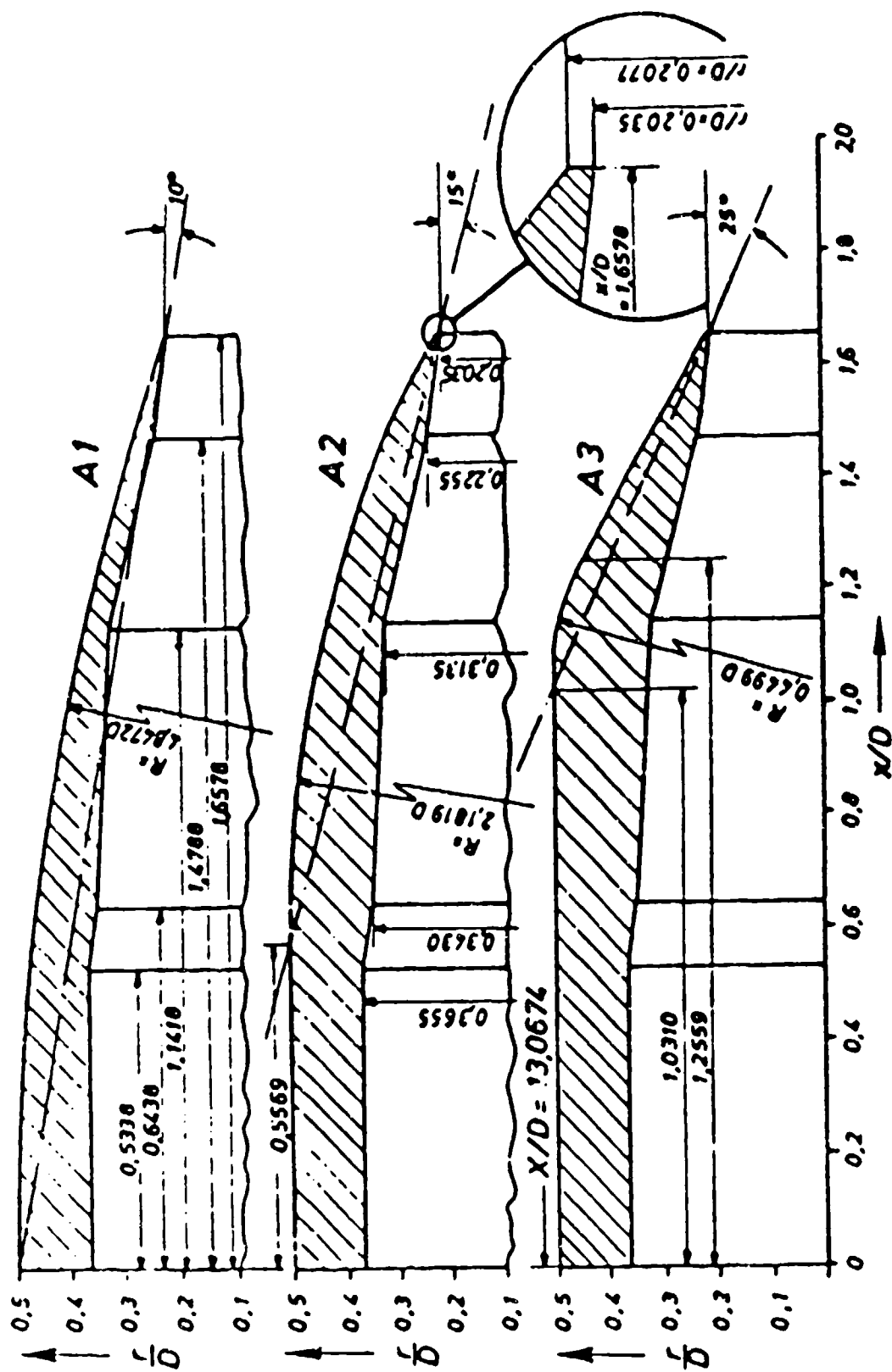
Geometric details of the bottled and nozzle contours of the AGARD-models

Figure 2b.
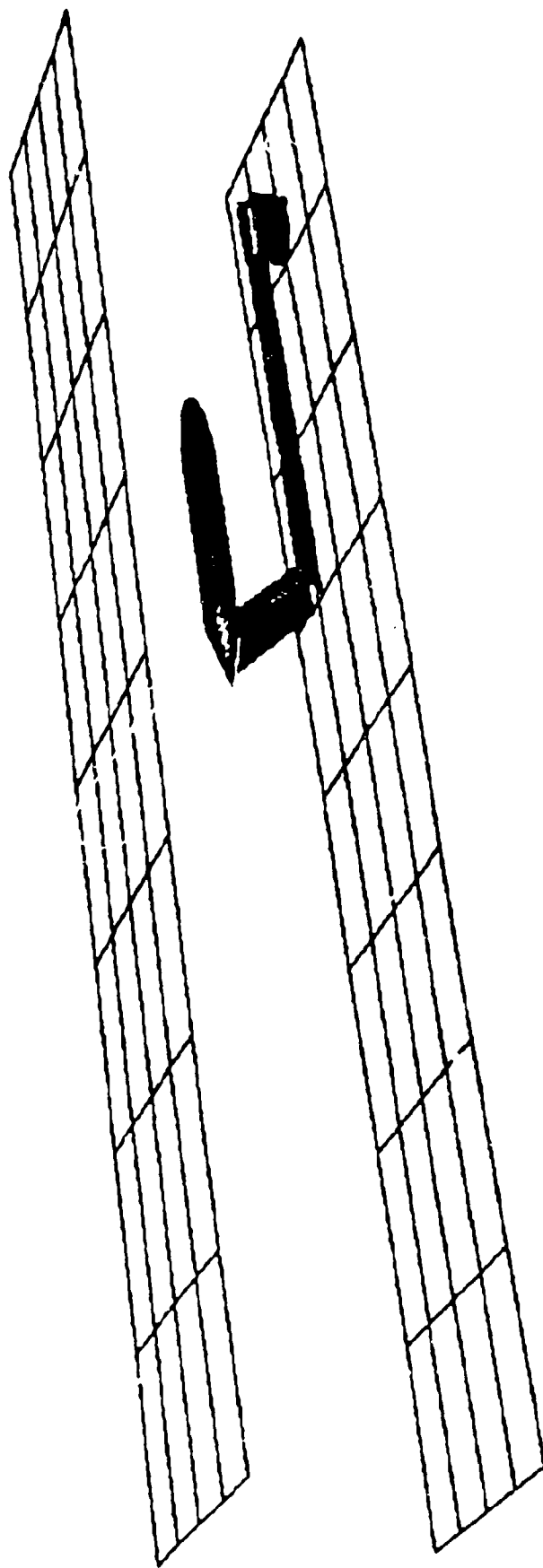
Figure 3. Computer Schematic of Model and Support Hardware, TGF Test
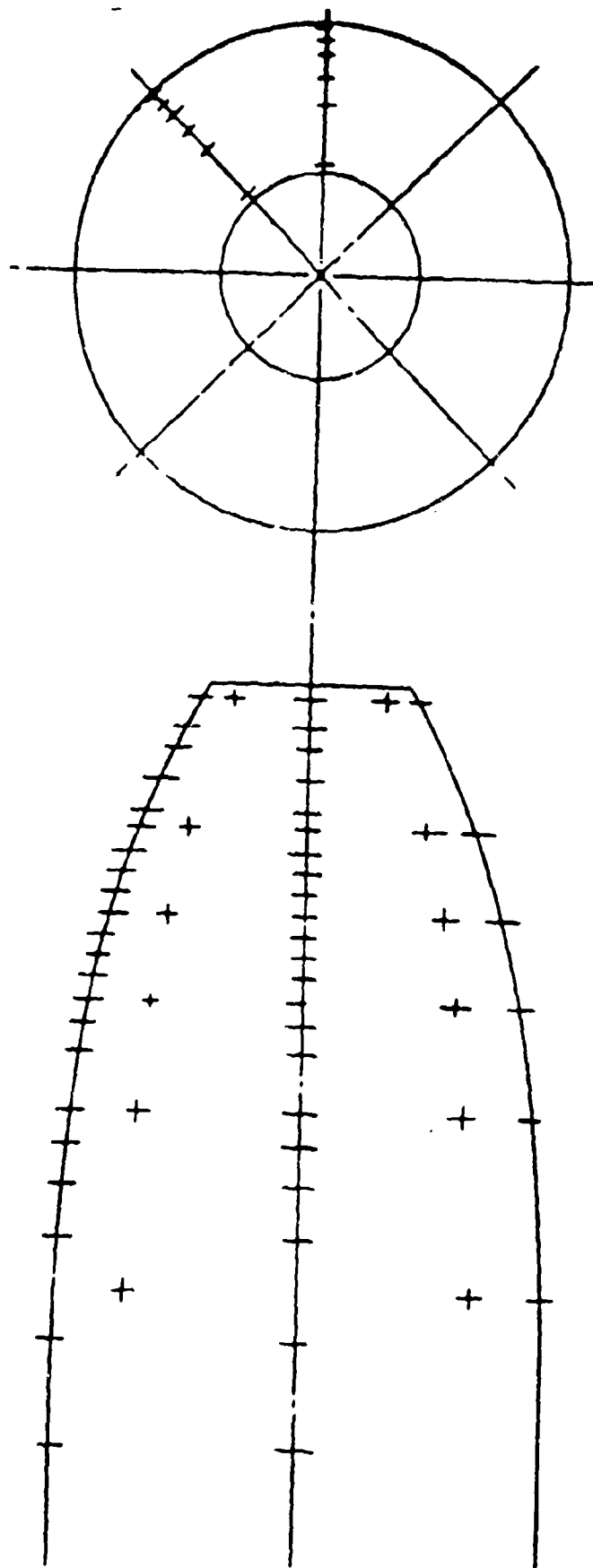
Figure 4. Nozzle Surface Tap Schedule, TGP Test
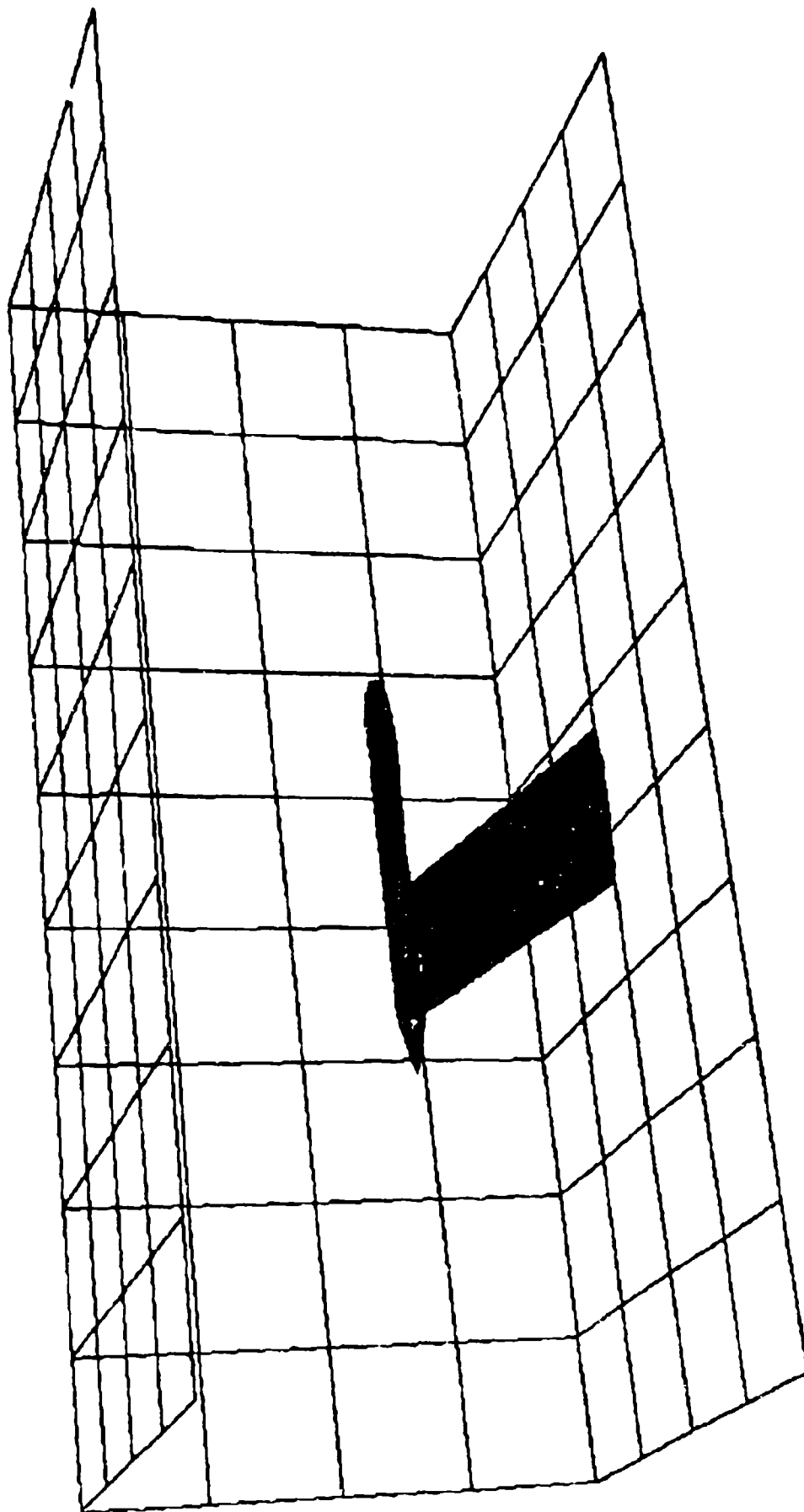
Figure 5. Computer Schematic of Model and Support Hardware, AEDC PWT 16T Test

Comparing Dimensions of TGF and 16T Models

16T subscale boattail model

(boattail)

(forebody)

2.98" dia

146.955"

TGF subscale boattail model

3.15" dia

30.119"

46.95"

Dotted lines represent the 16T model scaled down to the same boattail size as the TGF model (31.95% full size)
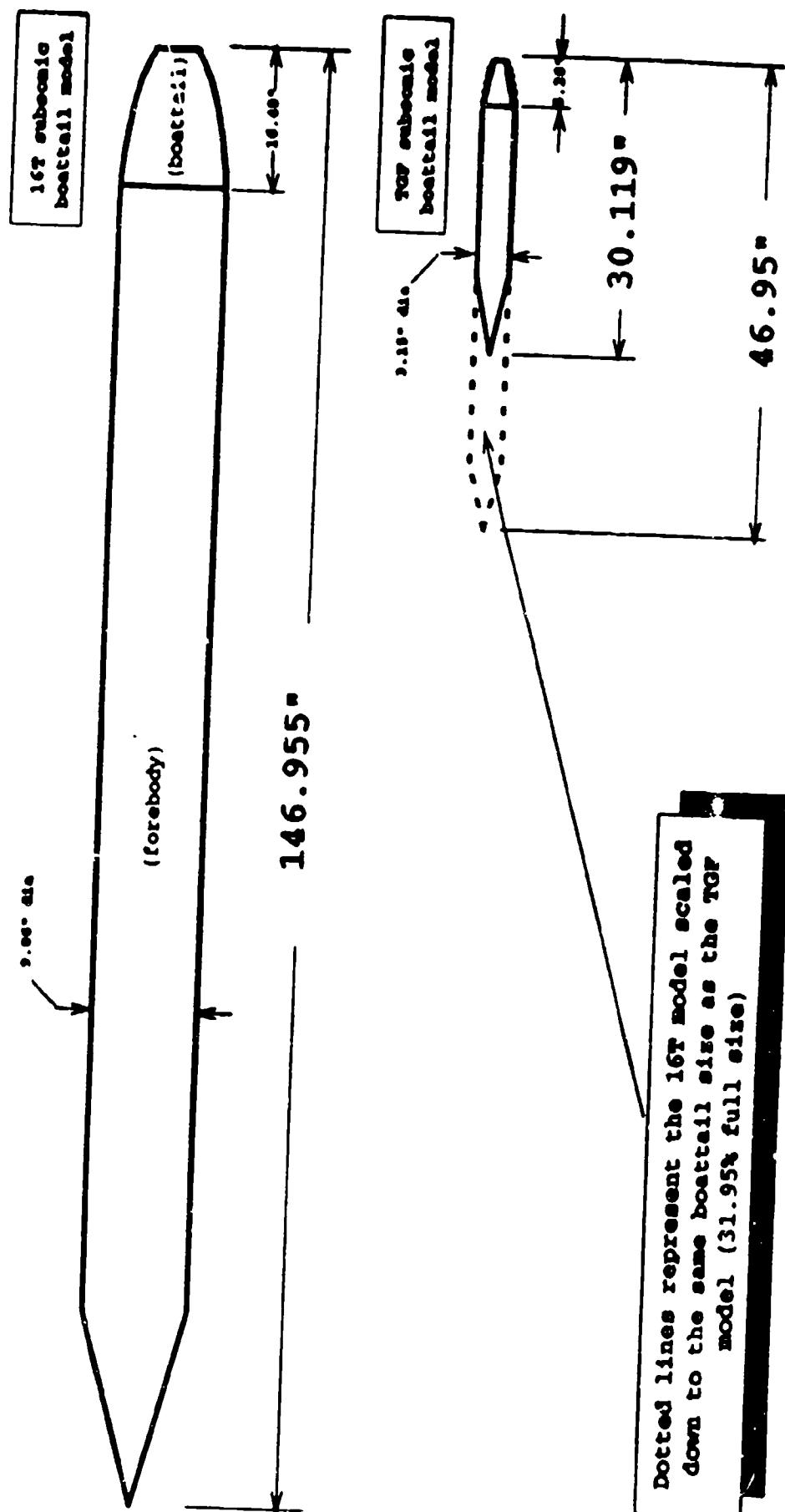
Figure 6. Comparing Dimensions of TGF and 16T Models
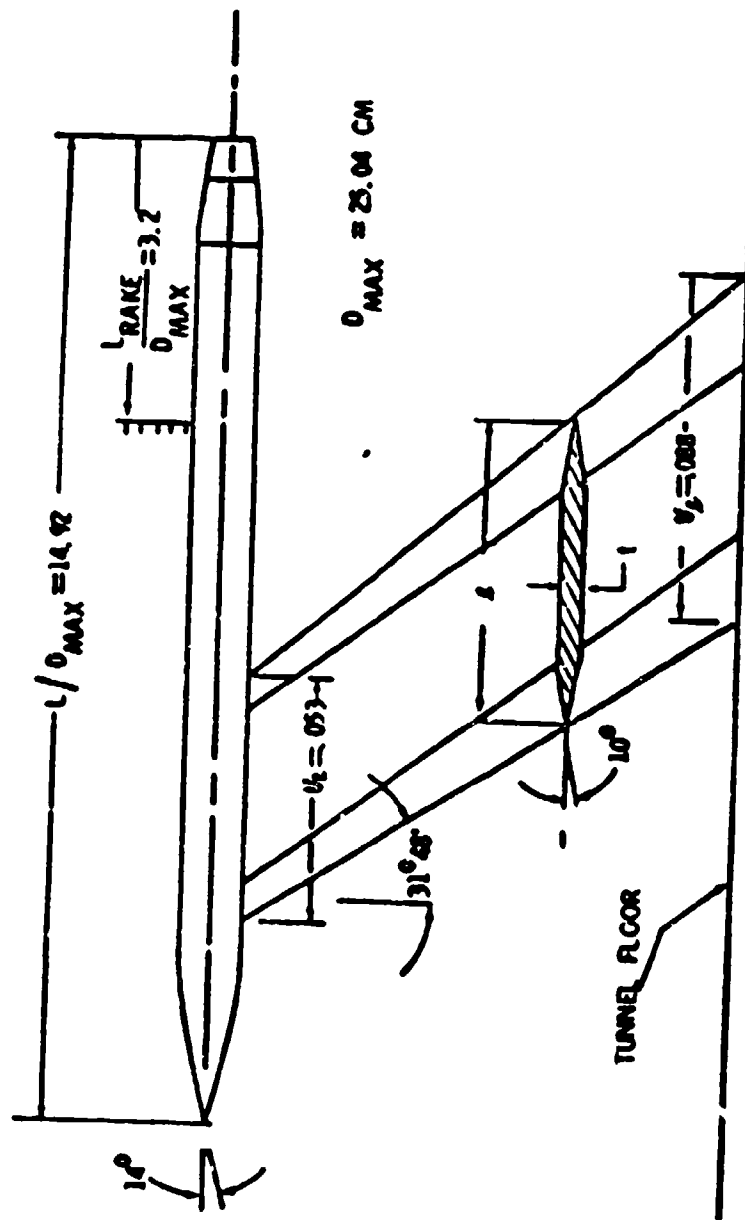
Figure 7. Dimensioned Drawing of 16T Model and Support Hardware

33

Tunnel/Test Body Specifics

	PWT 16T	TGF
Tunnel X-Section Area	256 ft^2	4 ft^2
Test Section Length	40 ft	6.08 ft
Maximum Model Diameter	.8217 ft	.2625 ft
Model Length	12.25 ft	2.51 ft
Boattail Length	1.37 ft	0.49 ft
Forebody Length	10.88 ft	2.02 ft
X-Section Blockage	0.207%	1.352%

Figure 8. Tunnel/Test Body Specifics

34

Summary Experimental Test Matrix

Mach Number	Re/ft	Pt/Ps
0.6	1.00e+06	1.276
0.6	1.50e+06	1.276
0.6	2.00e+06	1.276
0.6	2.50e+06	1.276
0.8	1.00e+06	1.524
0.8	1.50e+06	1.`4
0.8	2.00e+06	1...4
1.89	1.38e+06	6.700
1.89	2.07e+06	6.700
1.89	2.76e+06	6.700
1.89	4.00e+06	6.700
1.89	4.50e+06	6.700
2.3	1.38e+06	12.503
2.3	2.07e+06	12.503
2.3	2.76e+06	12.503
2.3	4.00e+06	12.503
2.3	4.50e+06	12.503
2.3	5.00e+06	12.503
3.0	1.38e+06	36.728
3.0	2.07e+06	36.728
3.0	2.76e+06	36.728
3.0	4.00e+06	36.728

Figure 9. Summary Experimental Test Matrix, TGF Test

CP COMPARISON WITH AEDC DATA
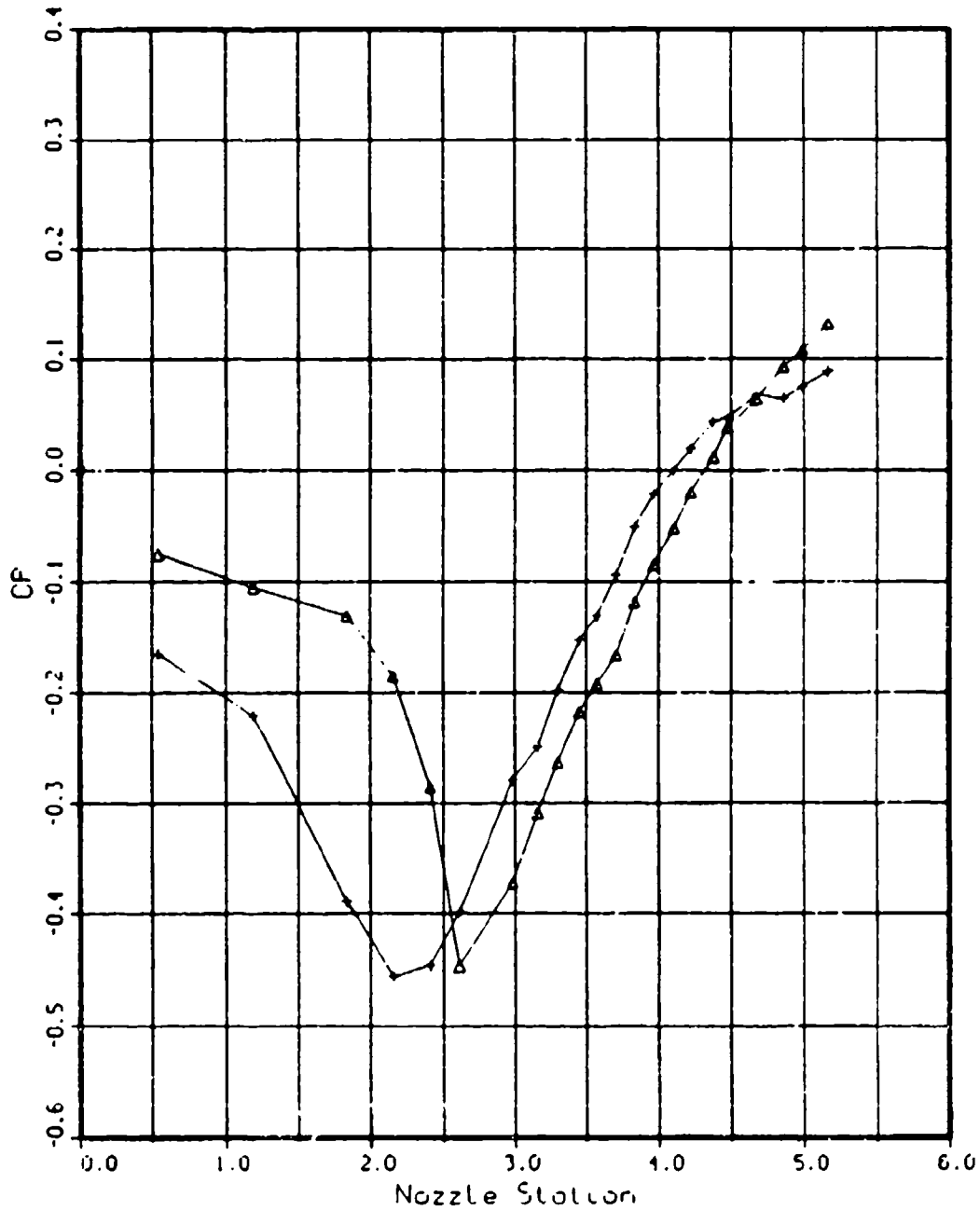
Figure 10. Sample CP Comparison With AEDC Data

36

10 Deg. Boattail, Mach 0.6, NPR 1.04

□   16T Experimental

△   TGF Experimental

Model Station (scaled to TGF stations in inches)

Cp
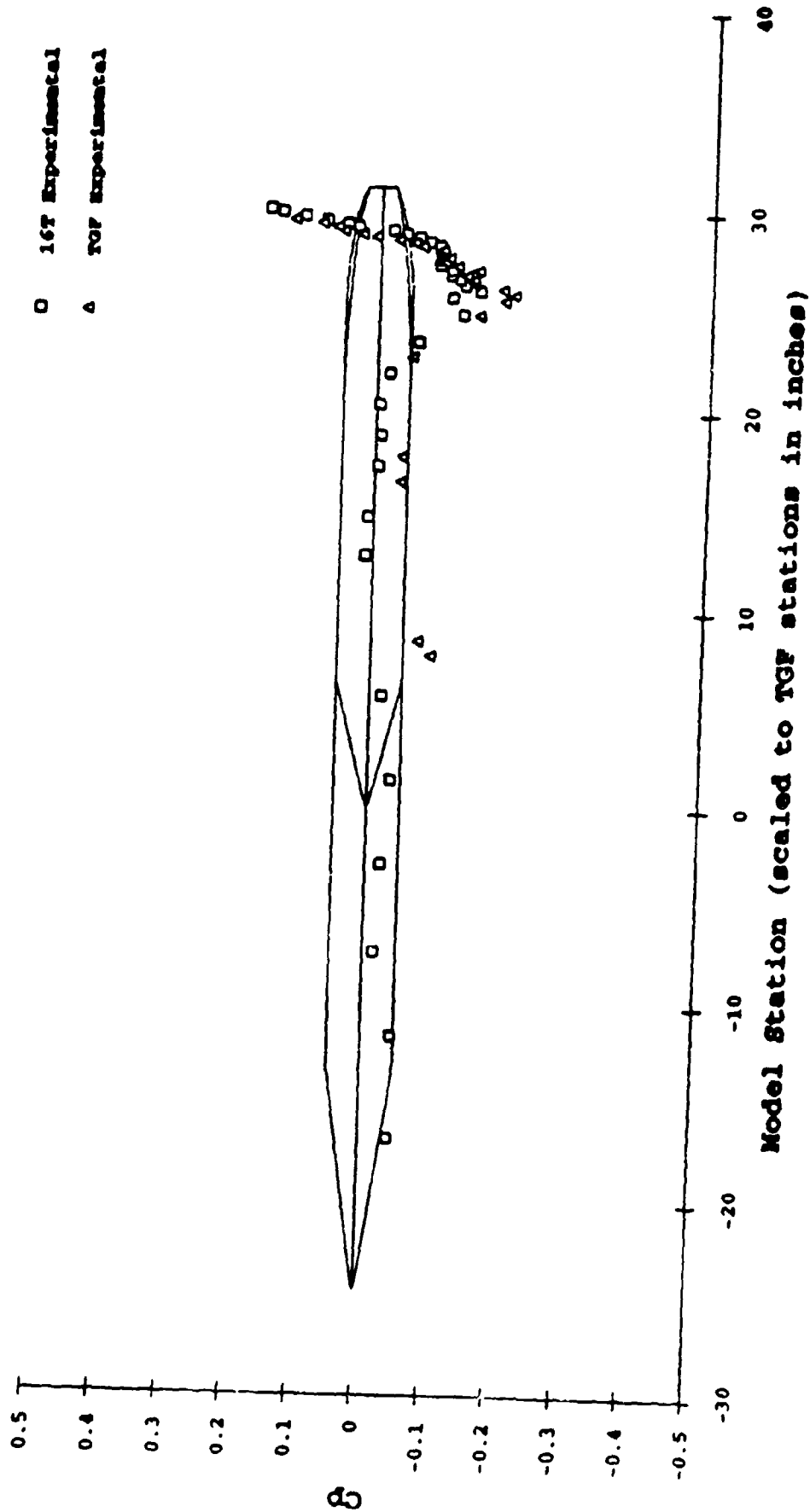
Figure 11(a). Comparison of Pressure Distributions Between Facilities

37

10 Deg. Boattail, Mach 0.6, NPR 3.00
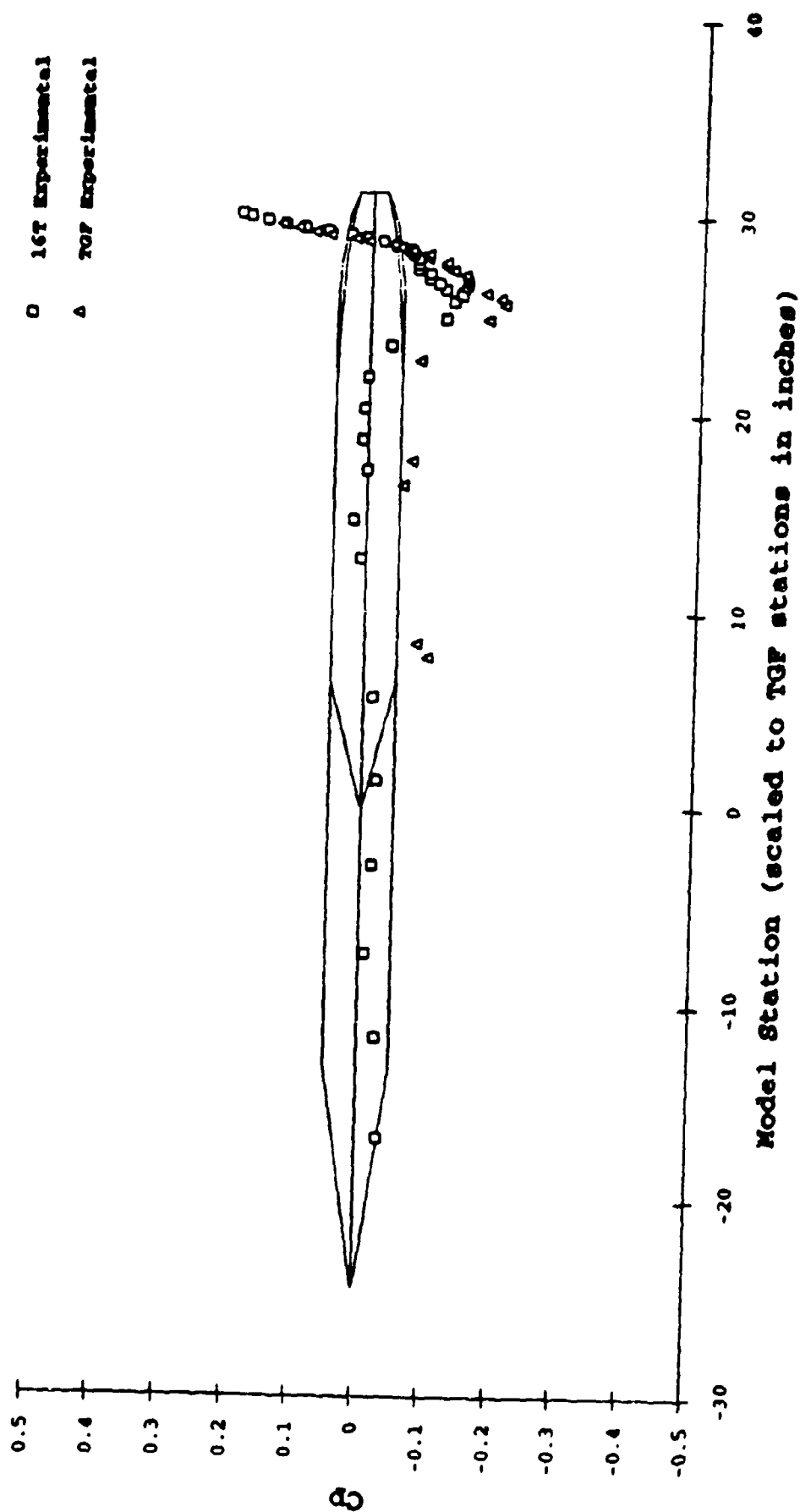
Figure 11(b). Comparison of Pressure Distributions Between Facilities
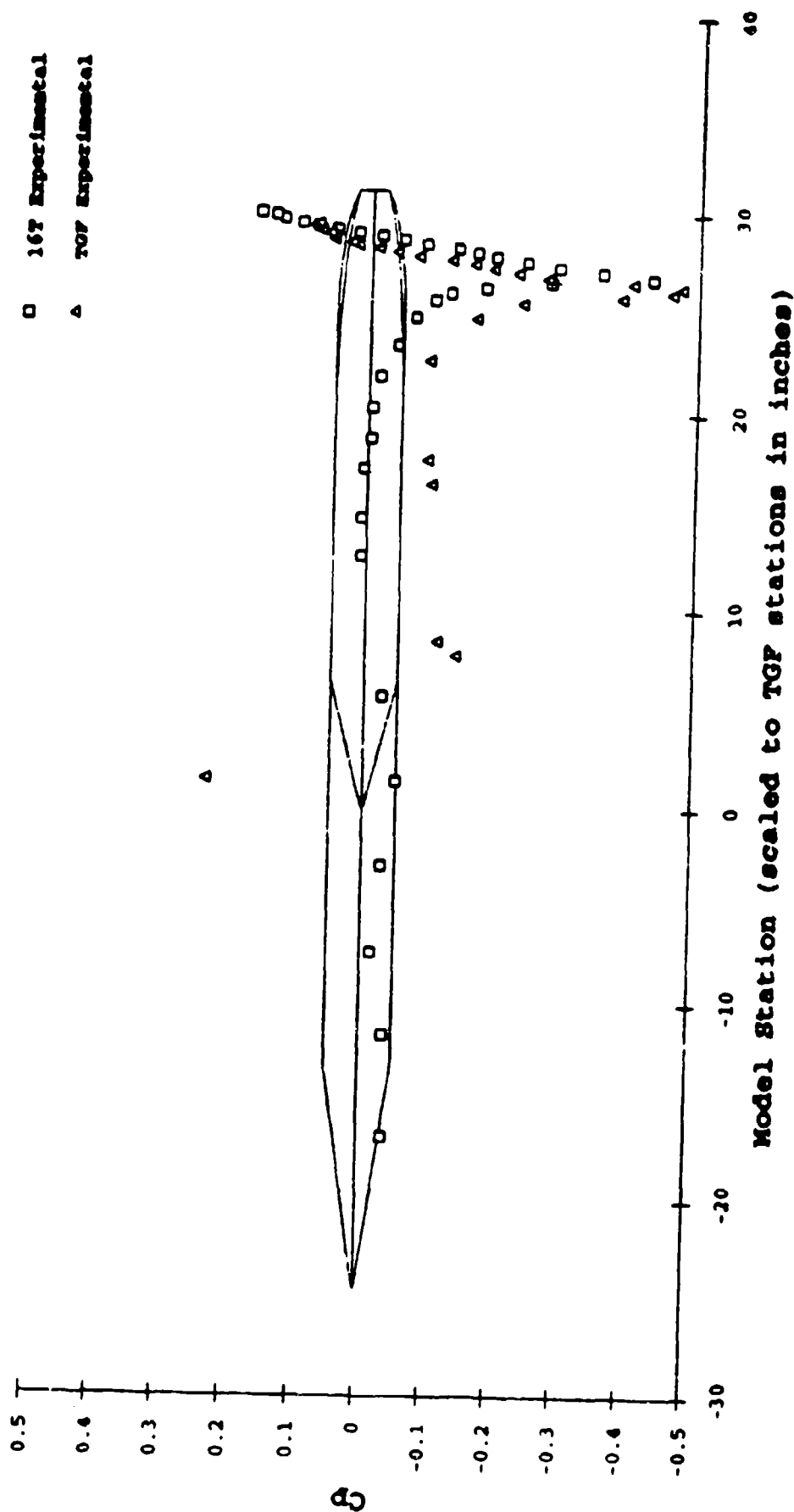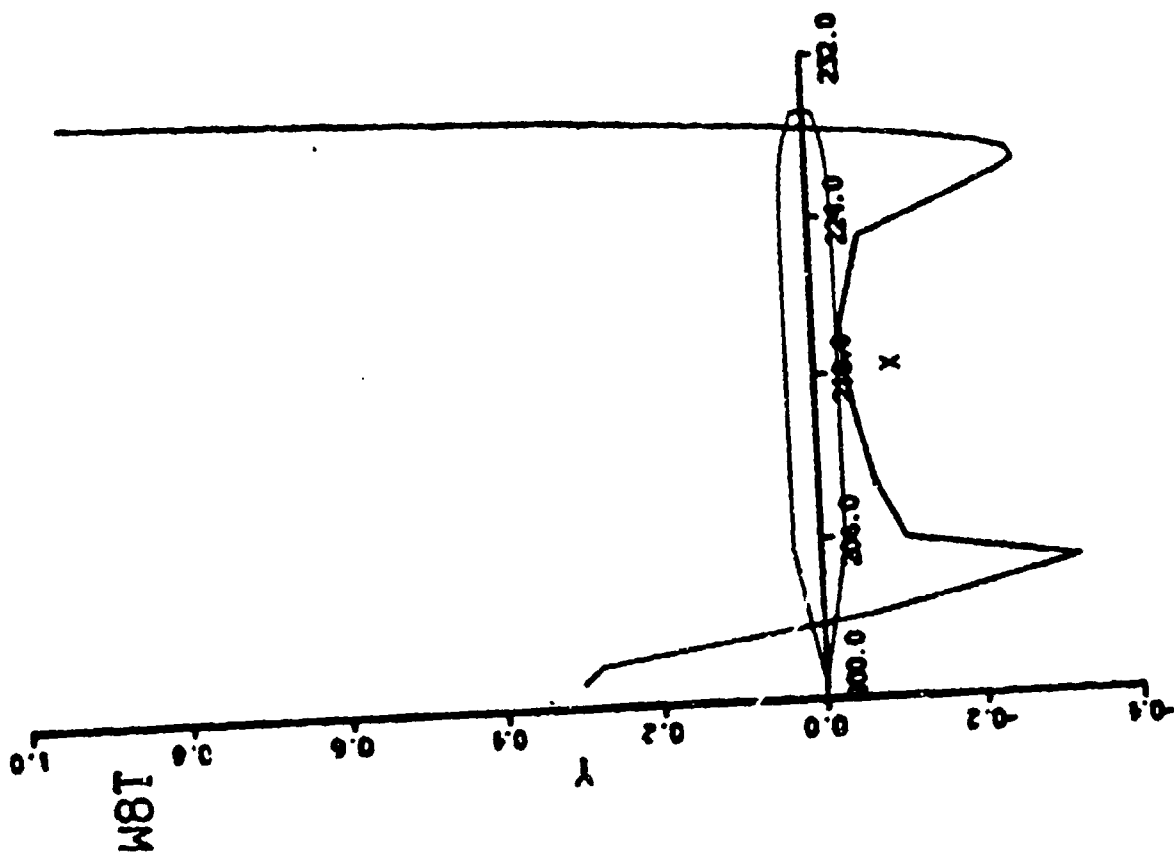
38

10 Deg. Boattail, Mach 0.8, NPR 1.04

16T Experimental □

TGF Experimental △

Model Station (scaled to TGF stations in inches)
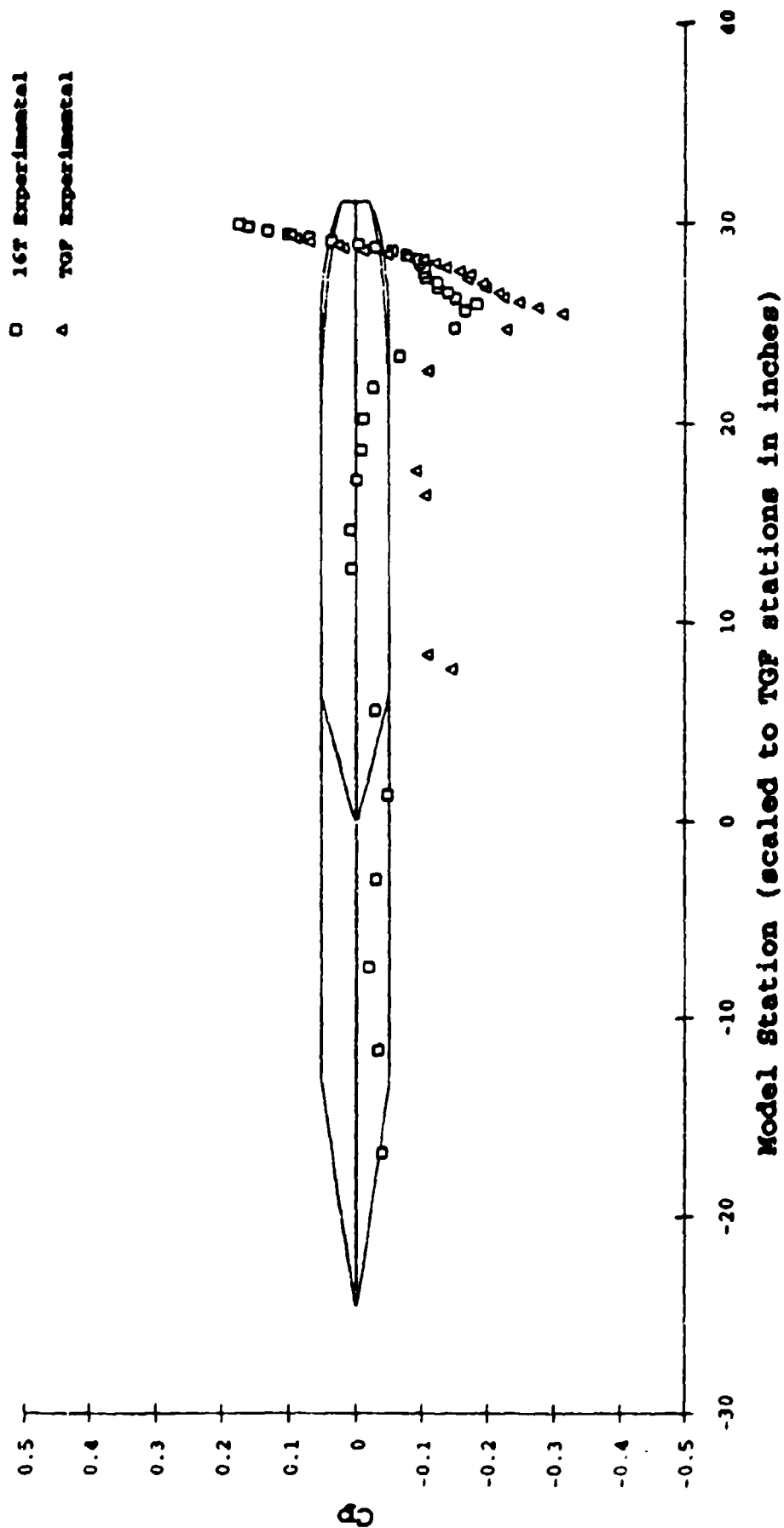
Figure 11(c). Comparison of Pressure Distributions Between Facilities

39

10 Deg. Boattail, Mach 0.8, NPR 3.00

□ 16T Experimental

△ TGF Experimental

CD

Model Station (scaled to TGF stations in inches)
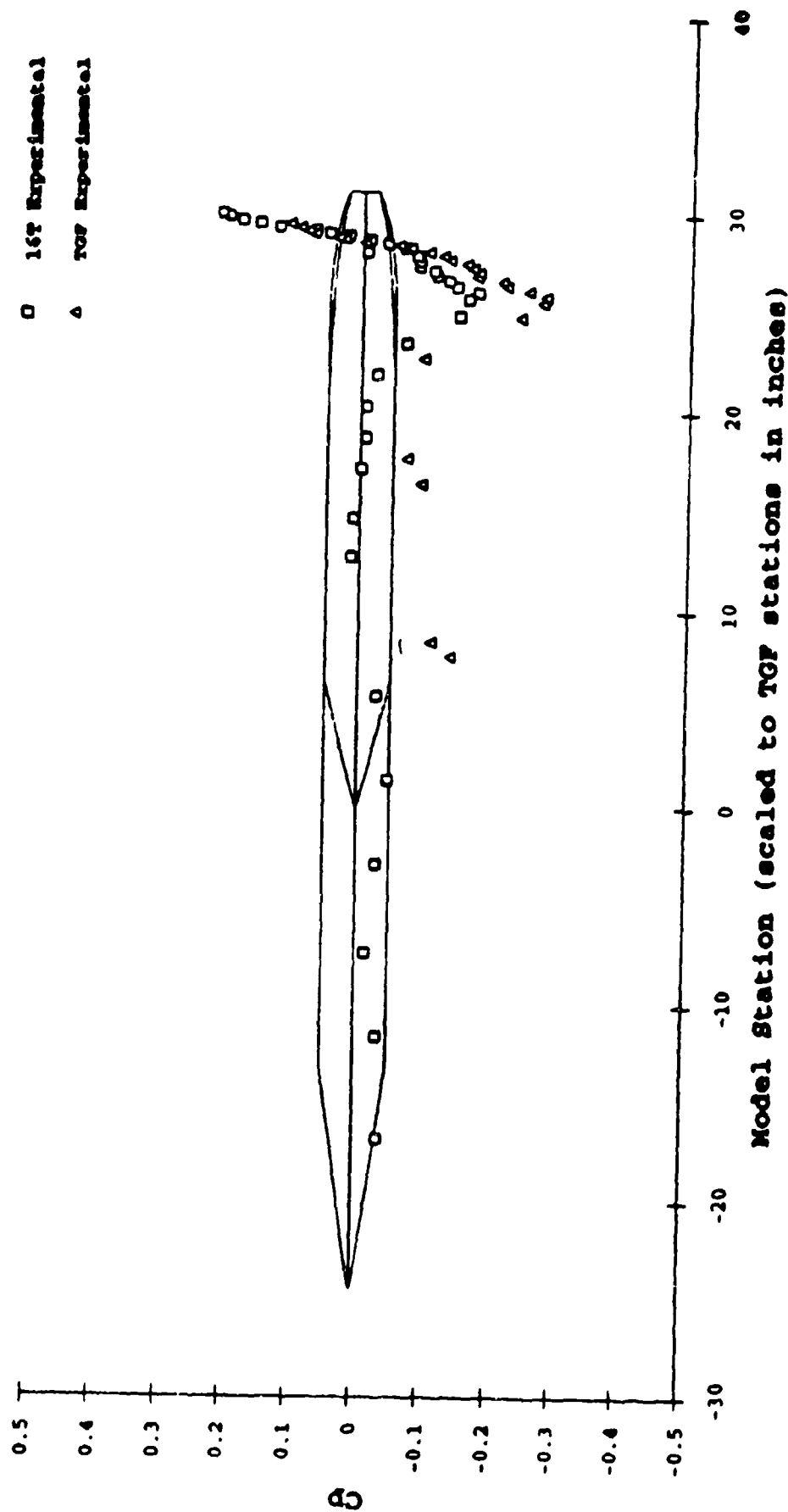
Figure 11(d). Comparison of Pressure Distributions Between Facilities

15 Deg. Boattail, Mach 0.6, NPR 1.04

□   16T Experimental

△   TGF Experimental

C_p

Model Station (scaled to TGF stations in inches)
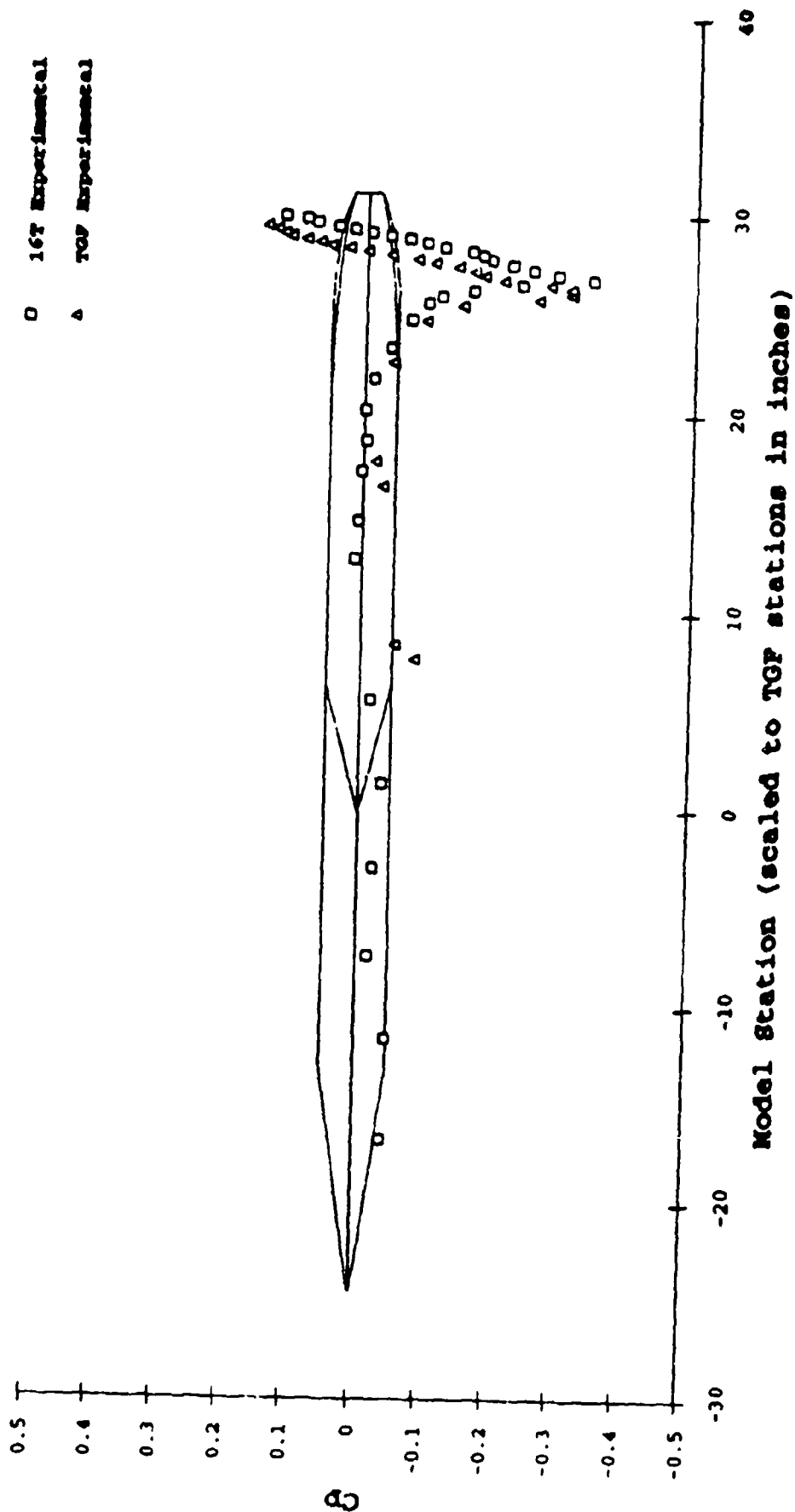
Figure 11(e). Comparison of Pressure Distributions Between Facilities

41

15 Deg. Boattail, Mach 0.6, NPR 3.00

Model Station (scaled to TGF stations in inches)
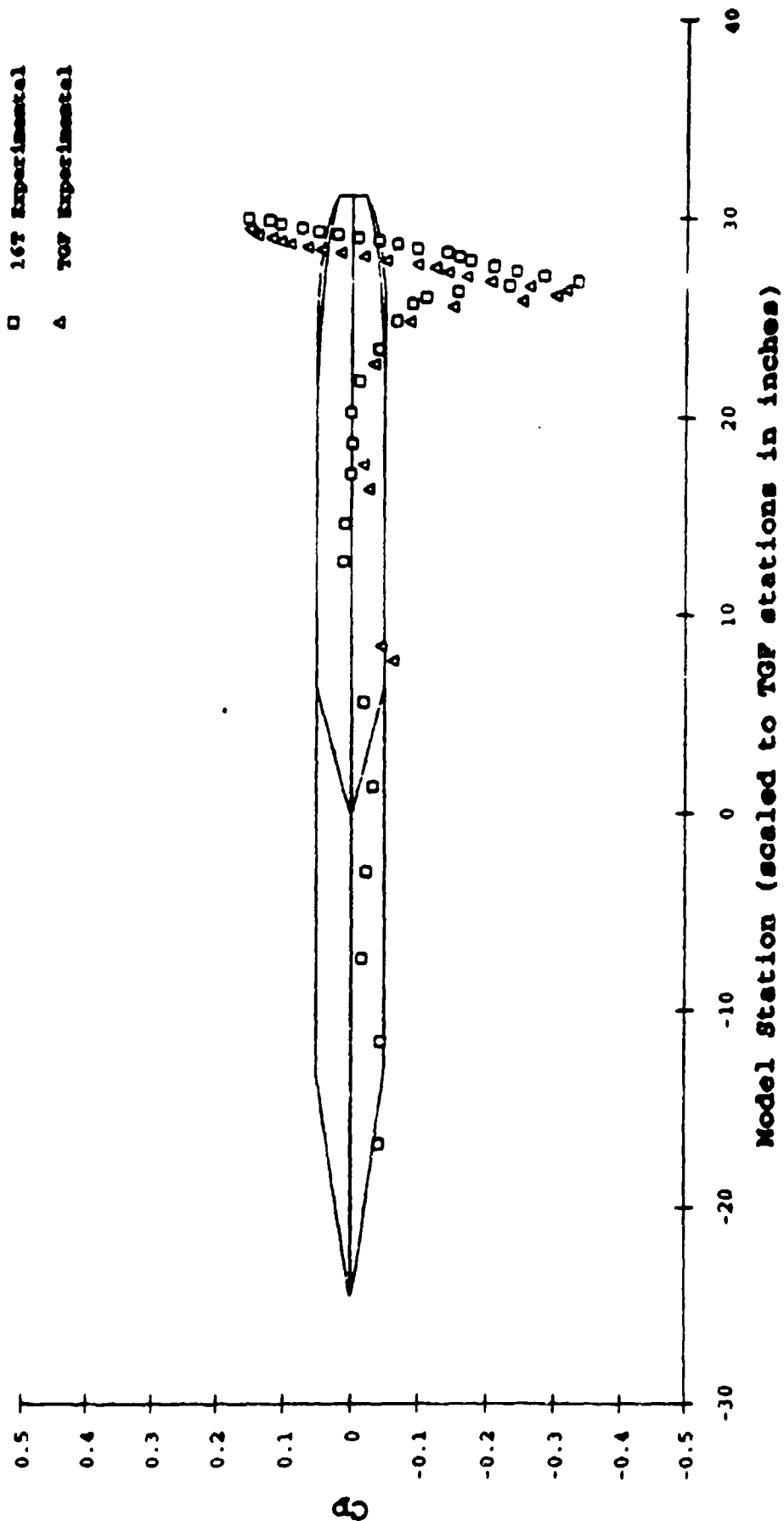
Figure 11(f). Comparison of Pressure Distributions Between Facilities

42

15 Deg. Boattail, Mach 0.8, NPR 1.04
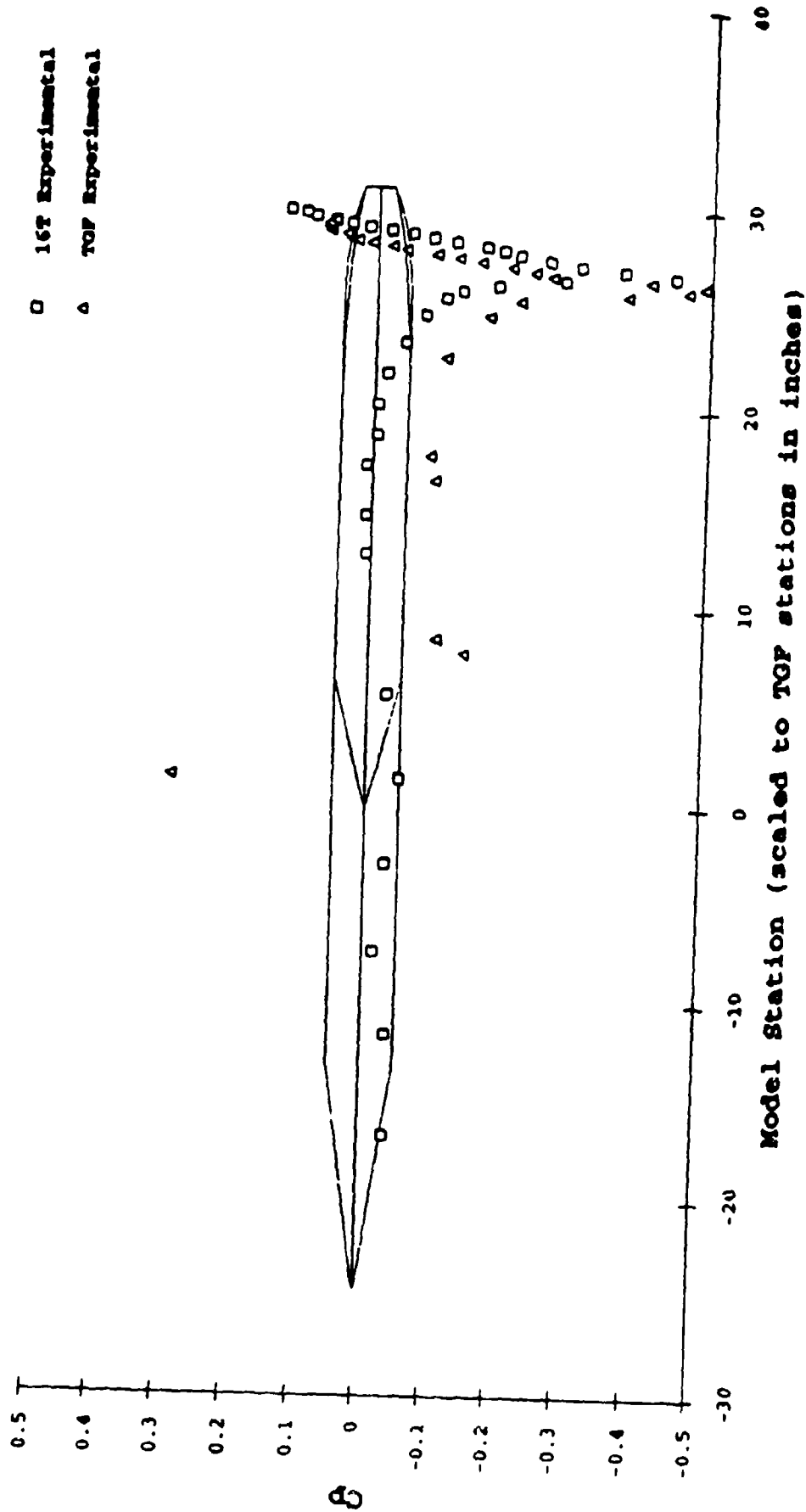
Figure 11(g). Comparison of Pressure Distributions Between Facilities

43

15 Deg. Boattail, Mach 0.8, NPR 3.00

□   16% Experimental

△   7% Experimental

Model Station (scaled to TGF stations in inches)

C_p

Figure 11(h). Comparison of Pressure Distributions Between Facilities

Figure 12. Sample Body/Boattail Pressure Distribution From Previous TGF Testing

10 Deg. Boattail, Mach 0.6, 16T Experimental Data
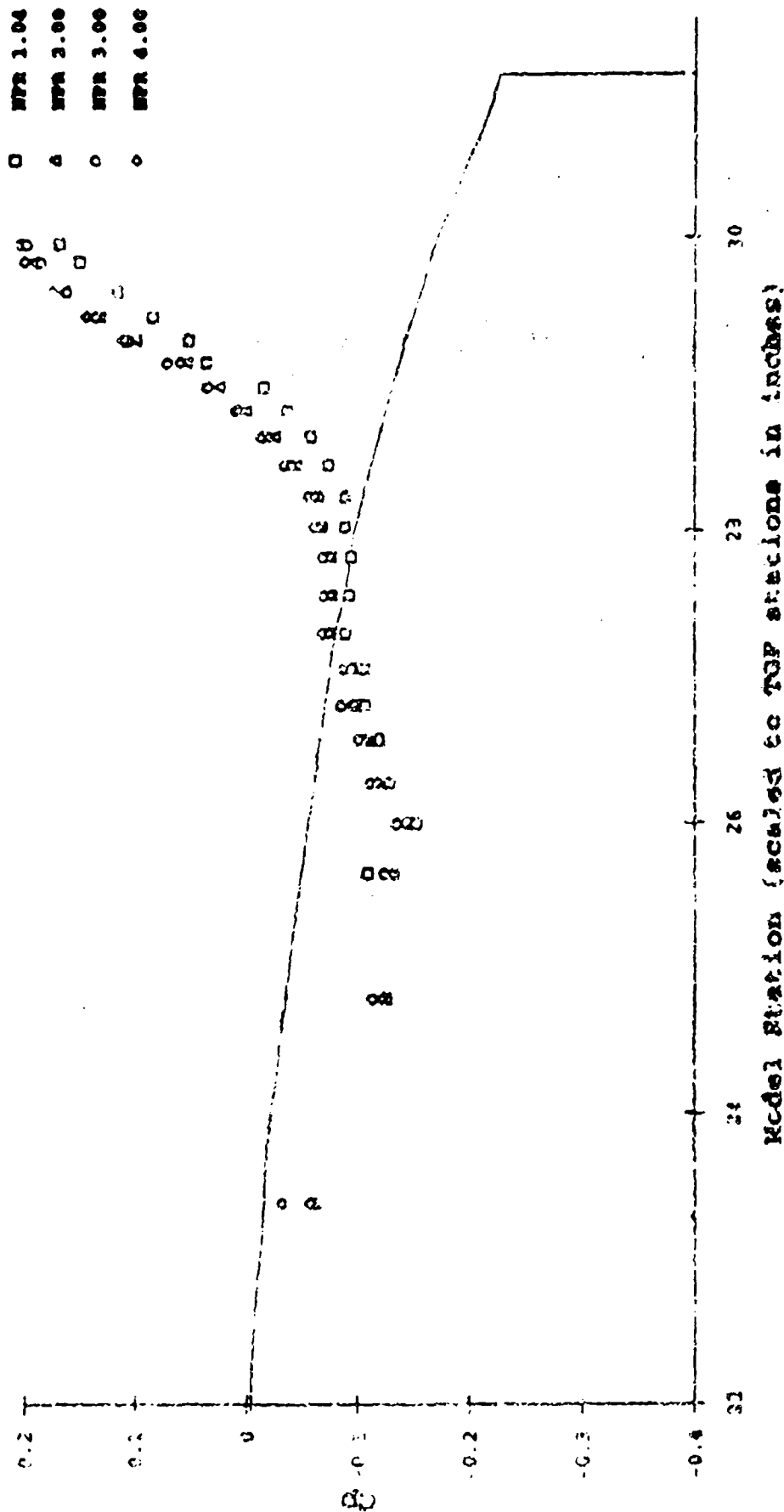
BPR 1.04
BPR 2.00
BPR 3.00
BPR 4.00

Model Station (scaled to TOP stations in inches)

Cp

Figure 13.? Comparison of Pressure Distributions Between NOWs Compared Incrementally Between Facilities

10 Deg. Boattail, Mach 0.6, TGF Experimental Data
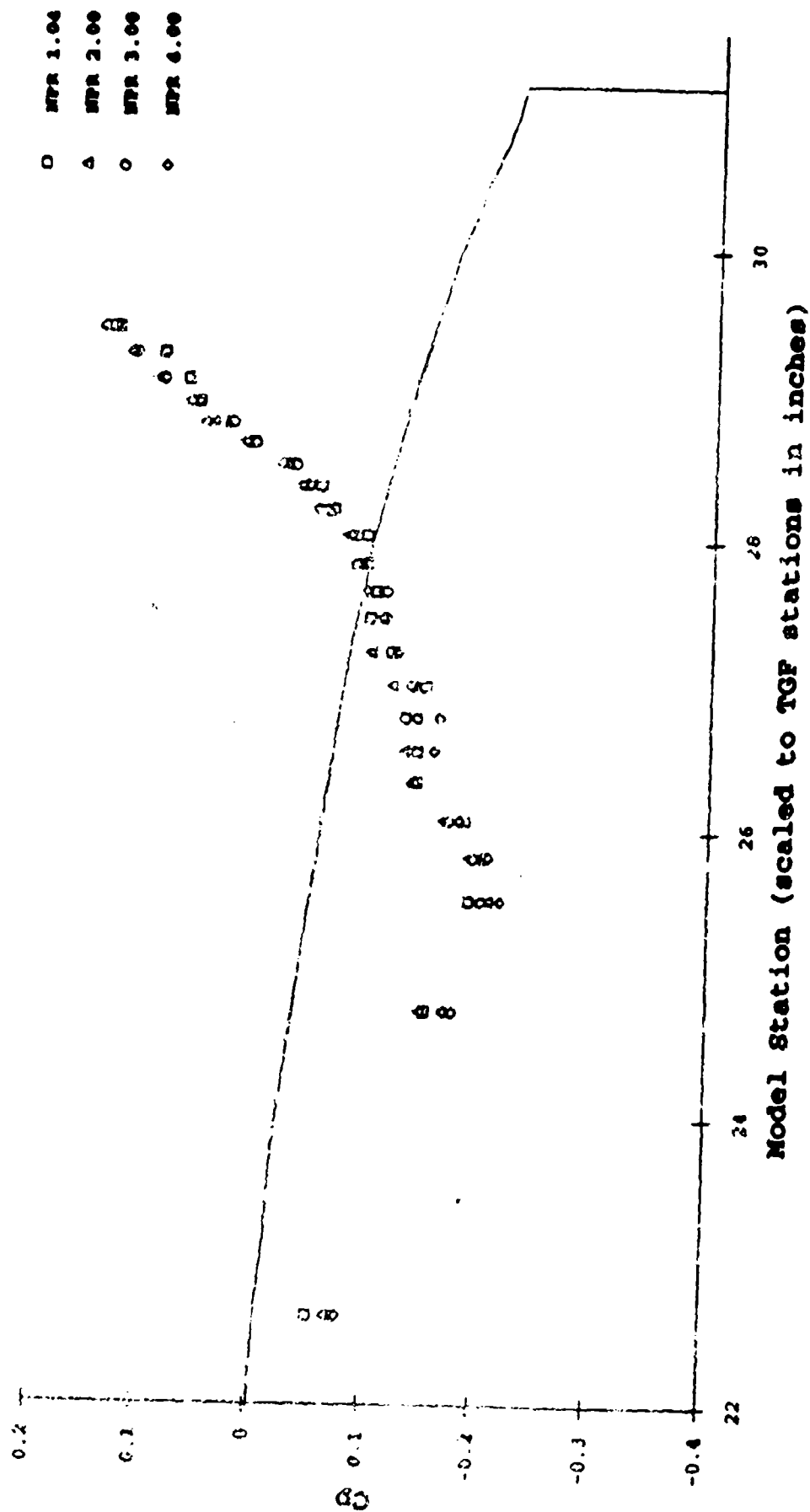
Figure 13(b). Comparison of Pressure Distributions Between NPRs Compared Incrementally Between Facilities
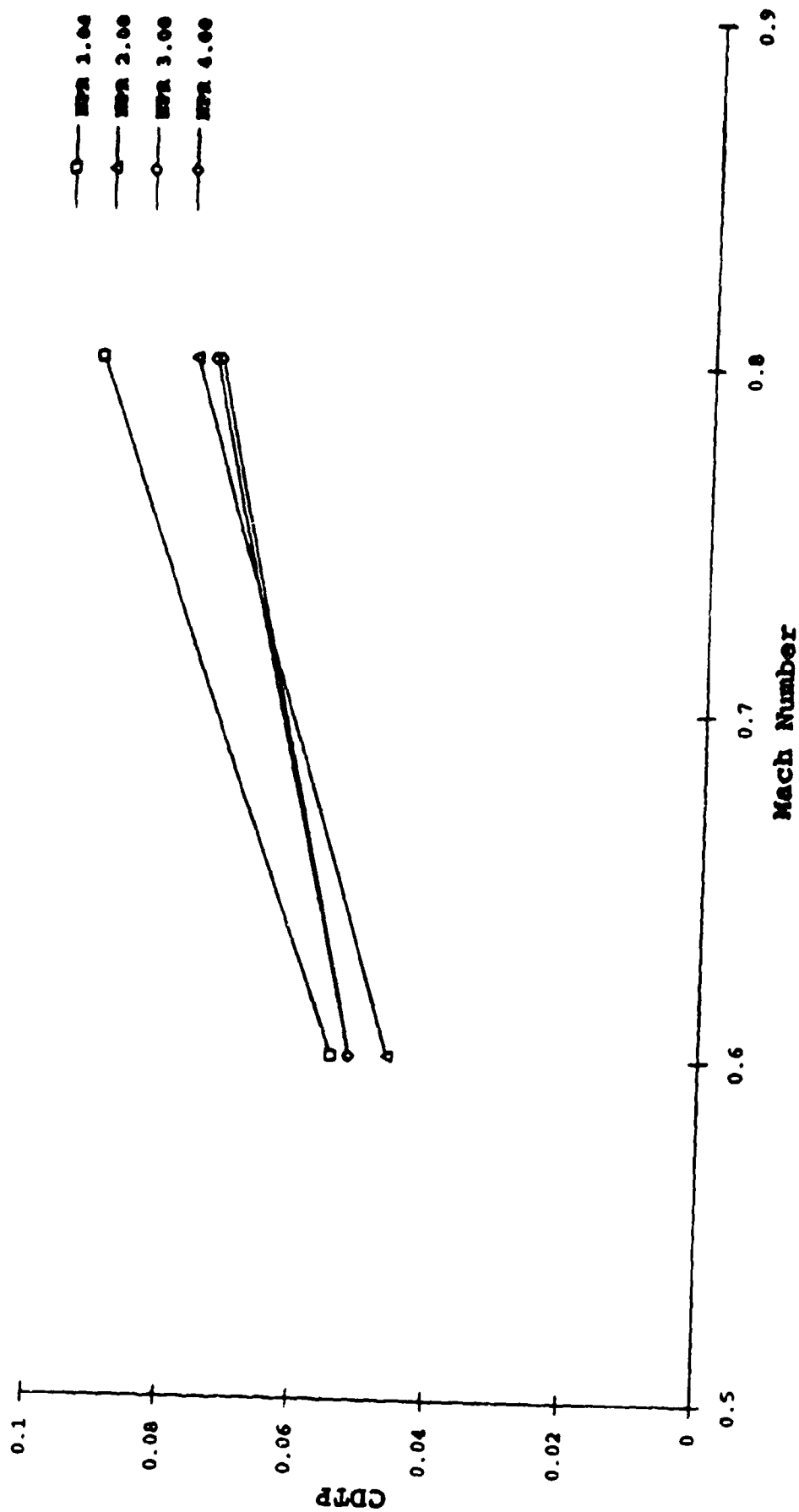
10 Deg. Boattail, Mach 0.8, 16T Experimental Data
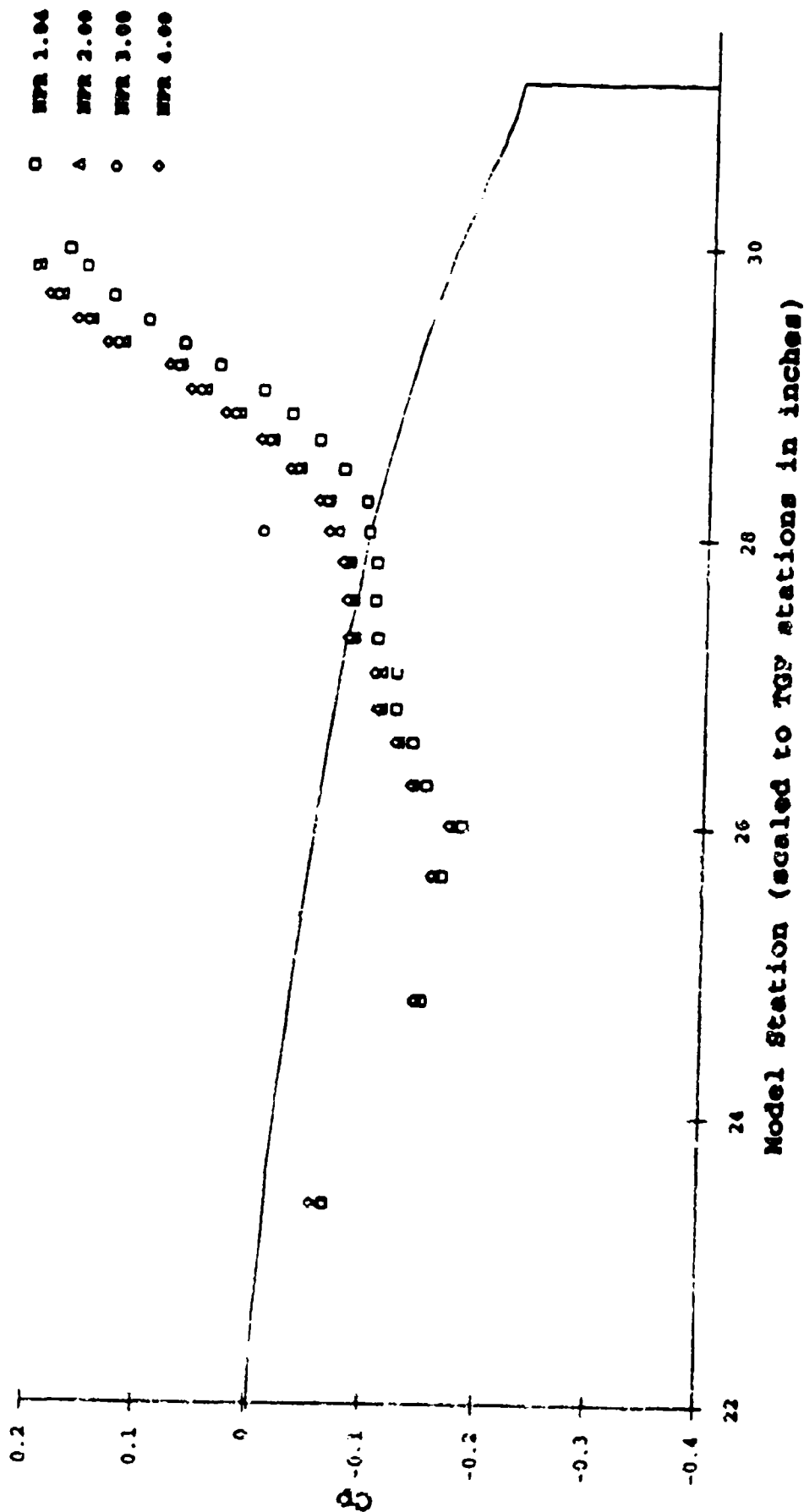
Figure 13(c). Comparison of Pressure Distributions Between NPRs Compared Incrementally Between Facilities

10 Deg. Boattail, Mach 0.8, TGF Experimental Data
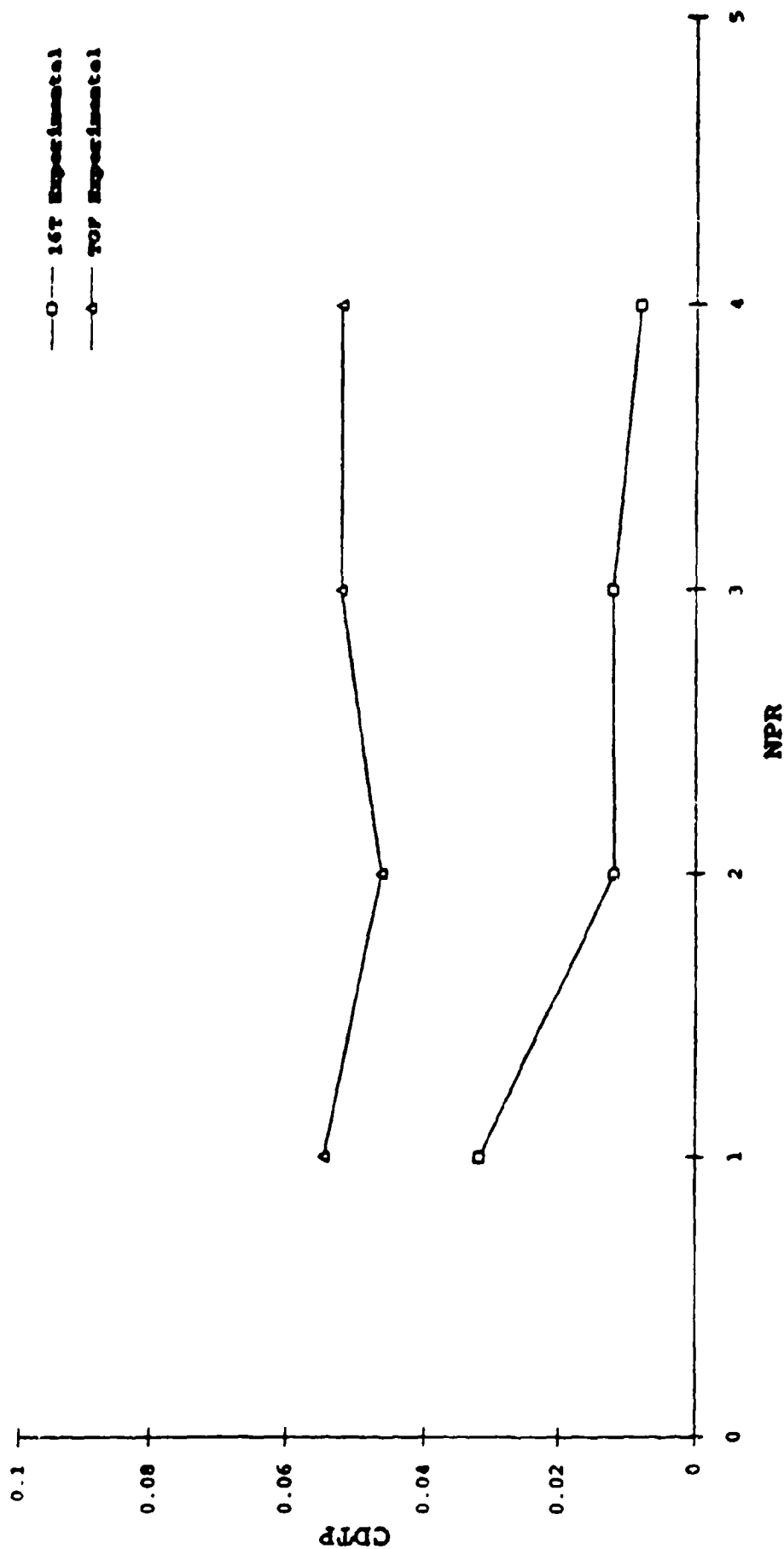
Model Station (scaled to TGF stations in inches)
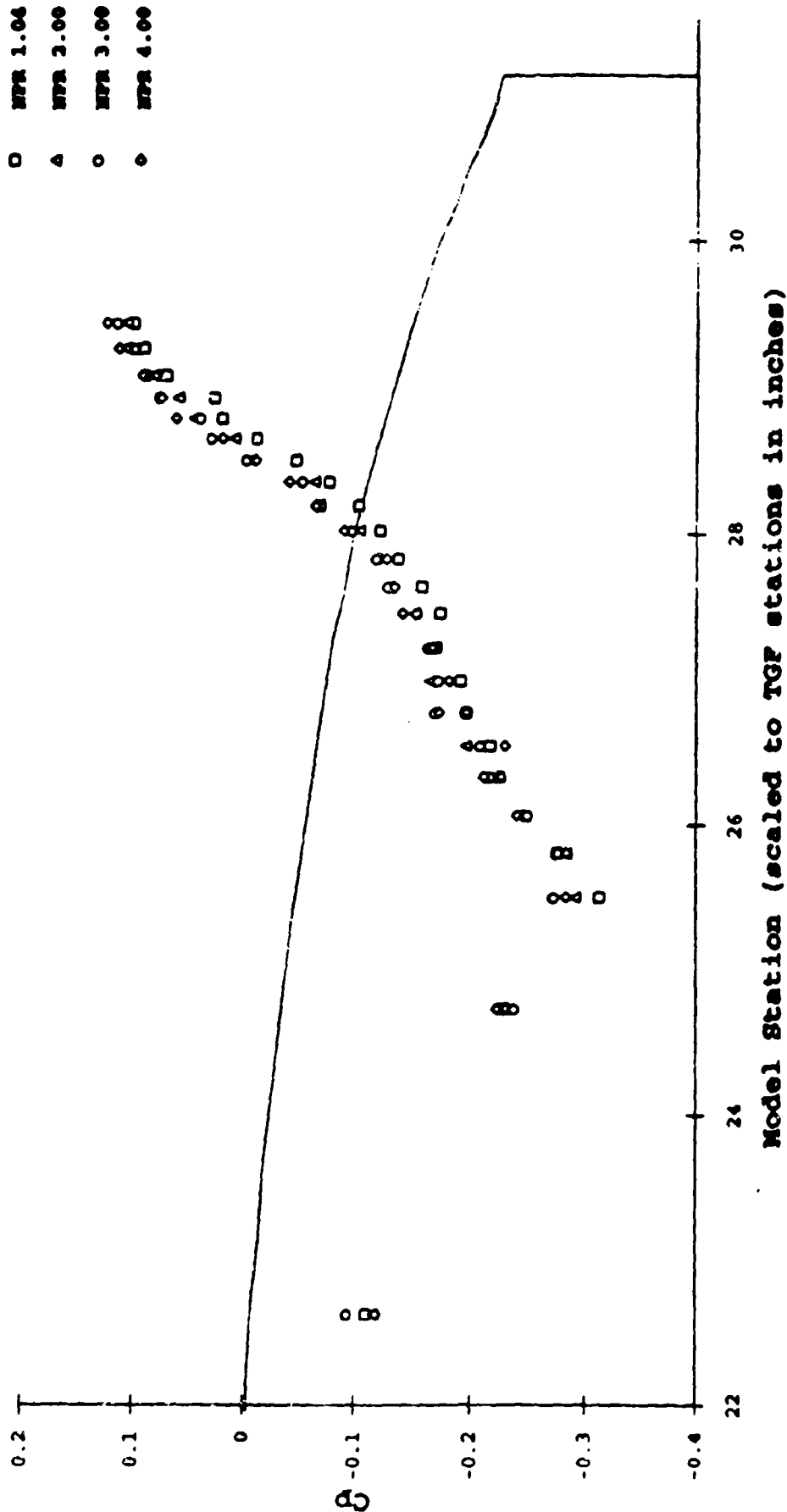
Figure 13(d). Comparison of Pressure Distributions Between NPRs Compared Incrementally Between Facilities

Mach 0.6, NPR 1.04, 16T Experimental Data
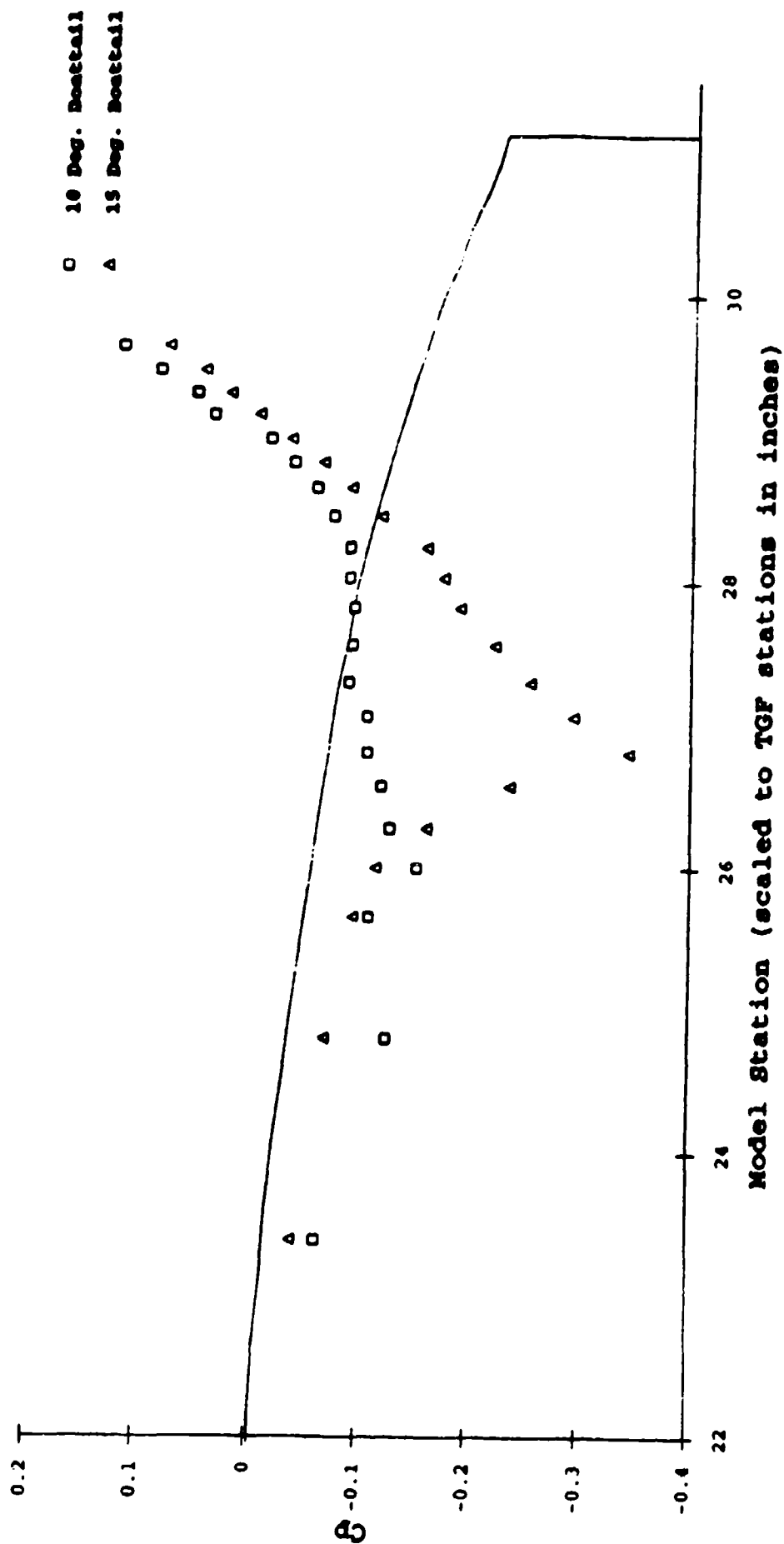
Figure 14(a). Comparison of Pressure Distributions Between Boattail Angles Compared Incrementally Between Facilities

50

Mach 0.6, NPR 1.04, TGF Experimental Data
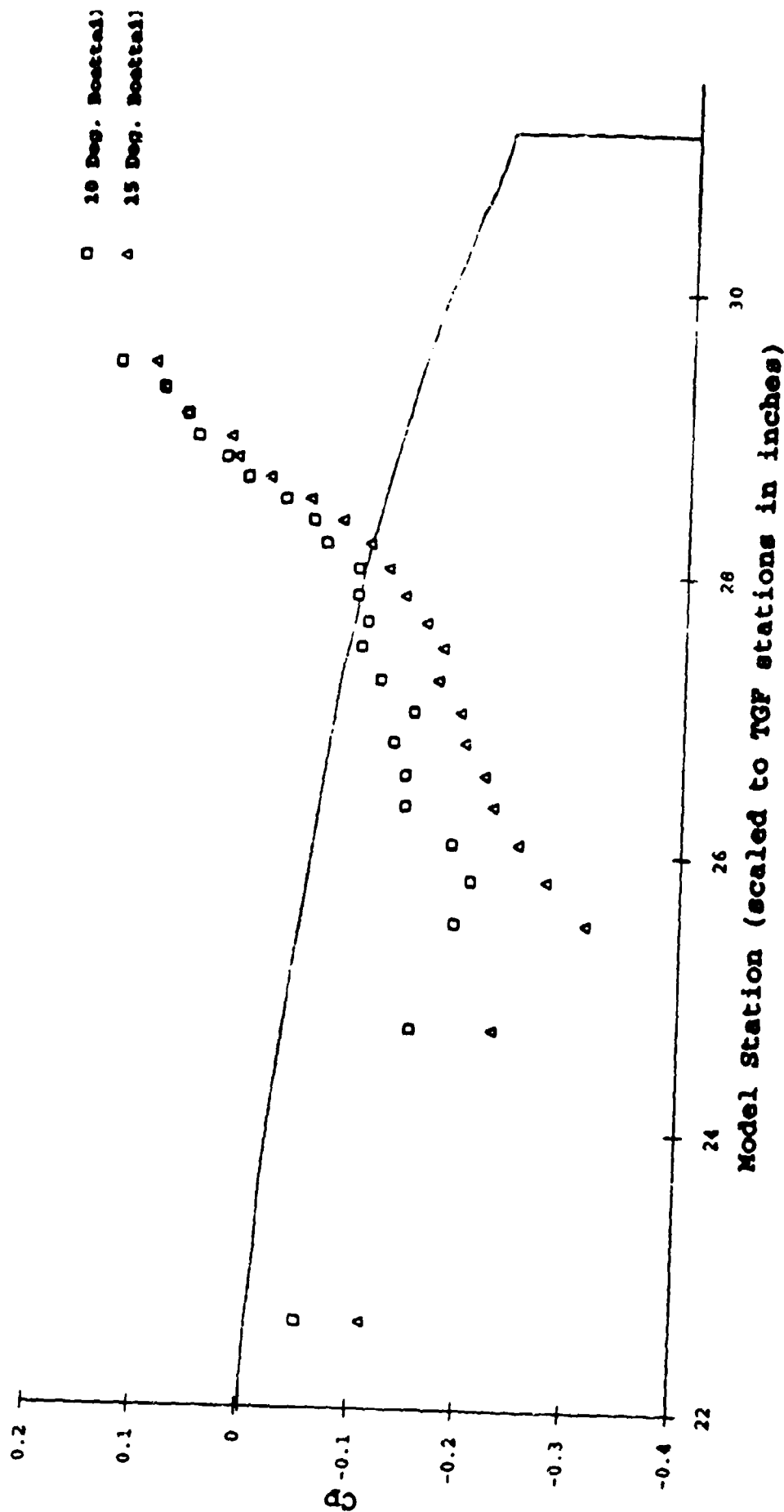
Figure 14(b). Comparison of Pressure Distributions Between Boattail Angles Compared Incrementally Between Facilities

51

10 Deg. Boattail, NPR 2.00
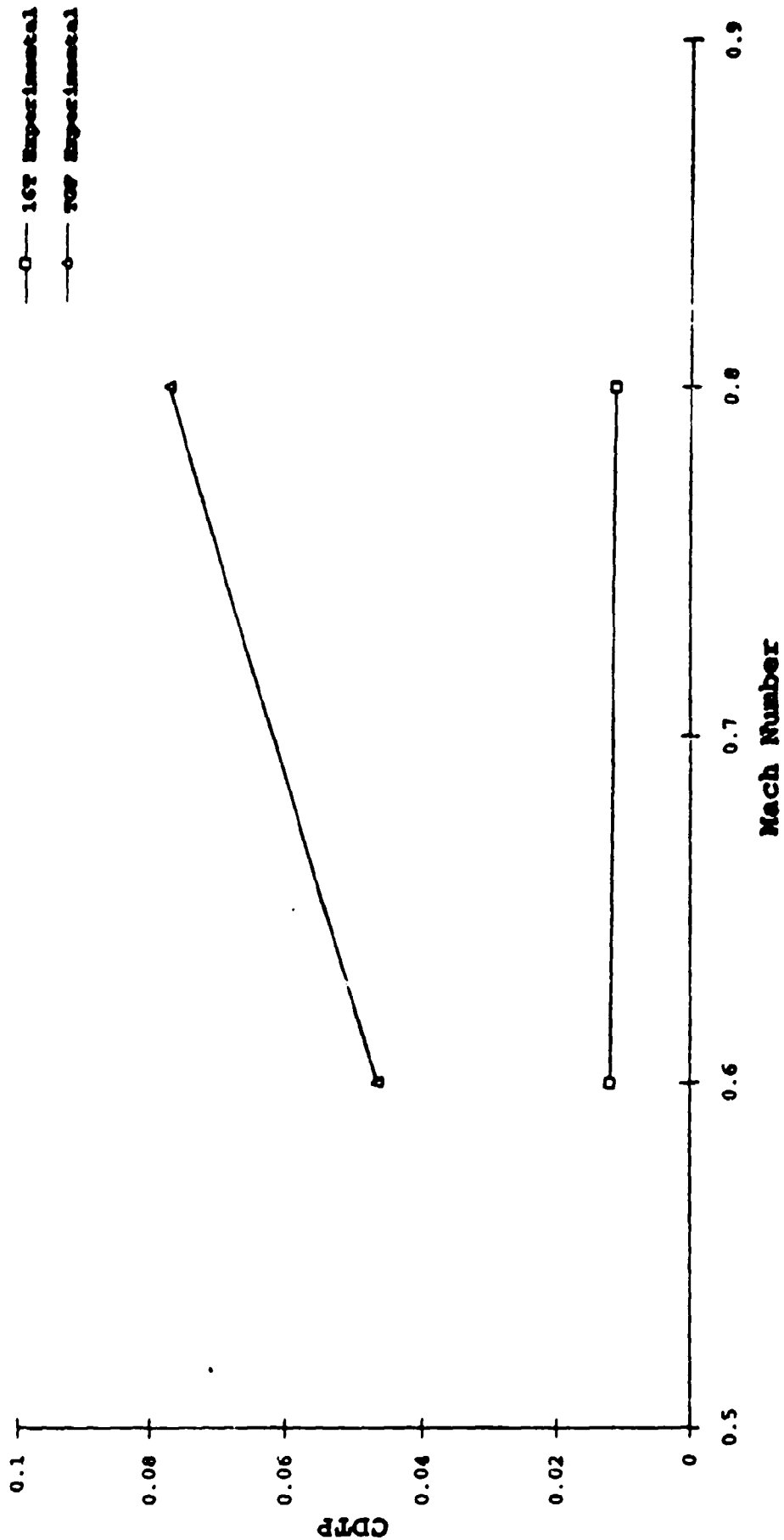
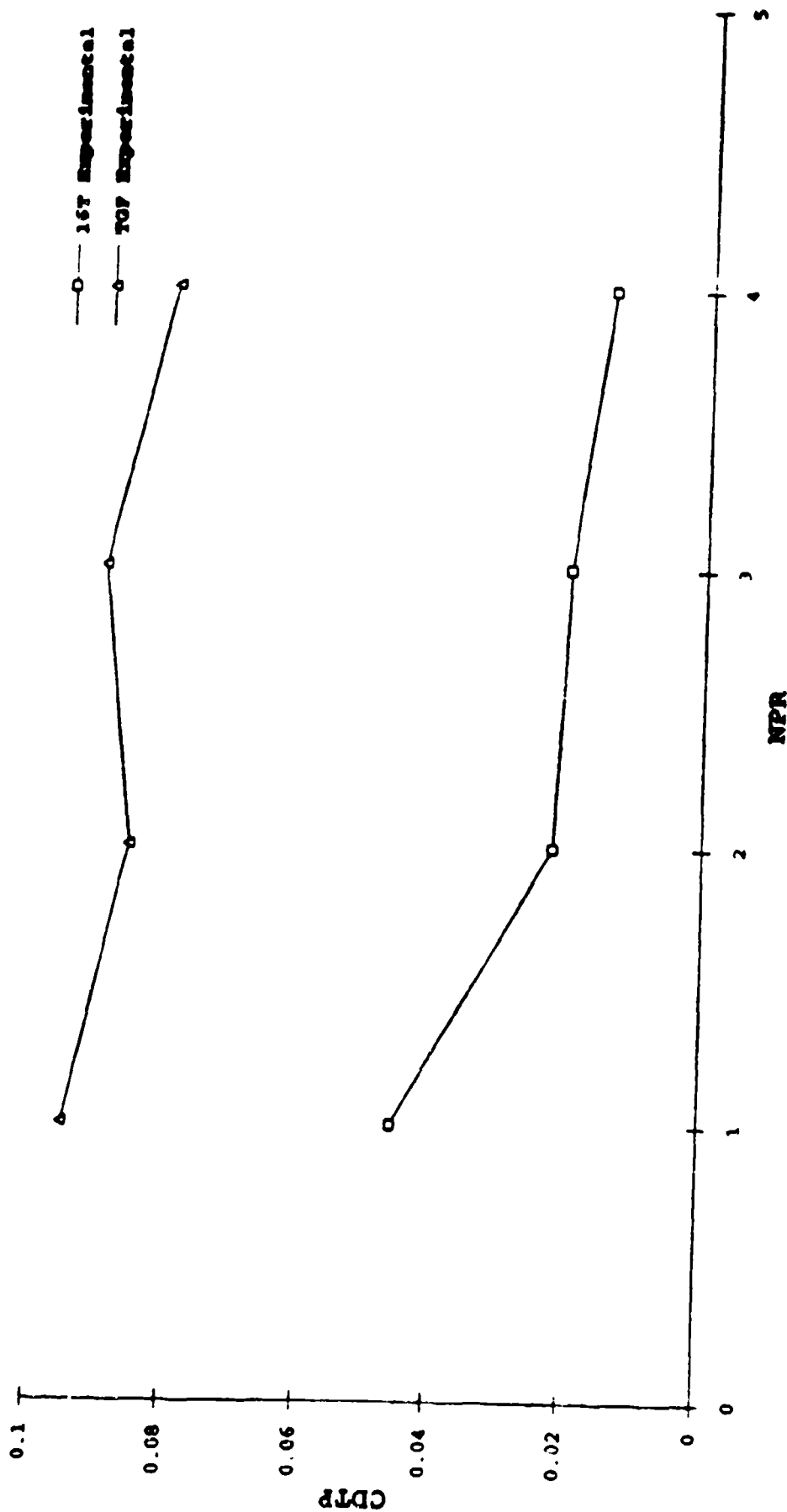Figure 15(a). Comparison of Pressure Drag Coefficients Between Facilities

10 Deg. Boattail, NPR 4.00
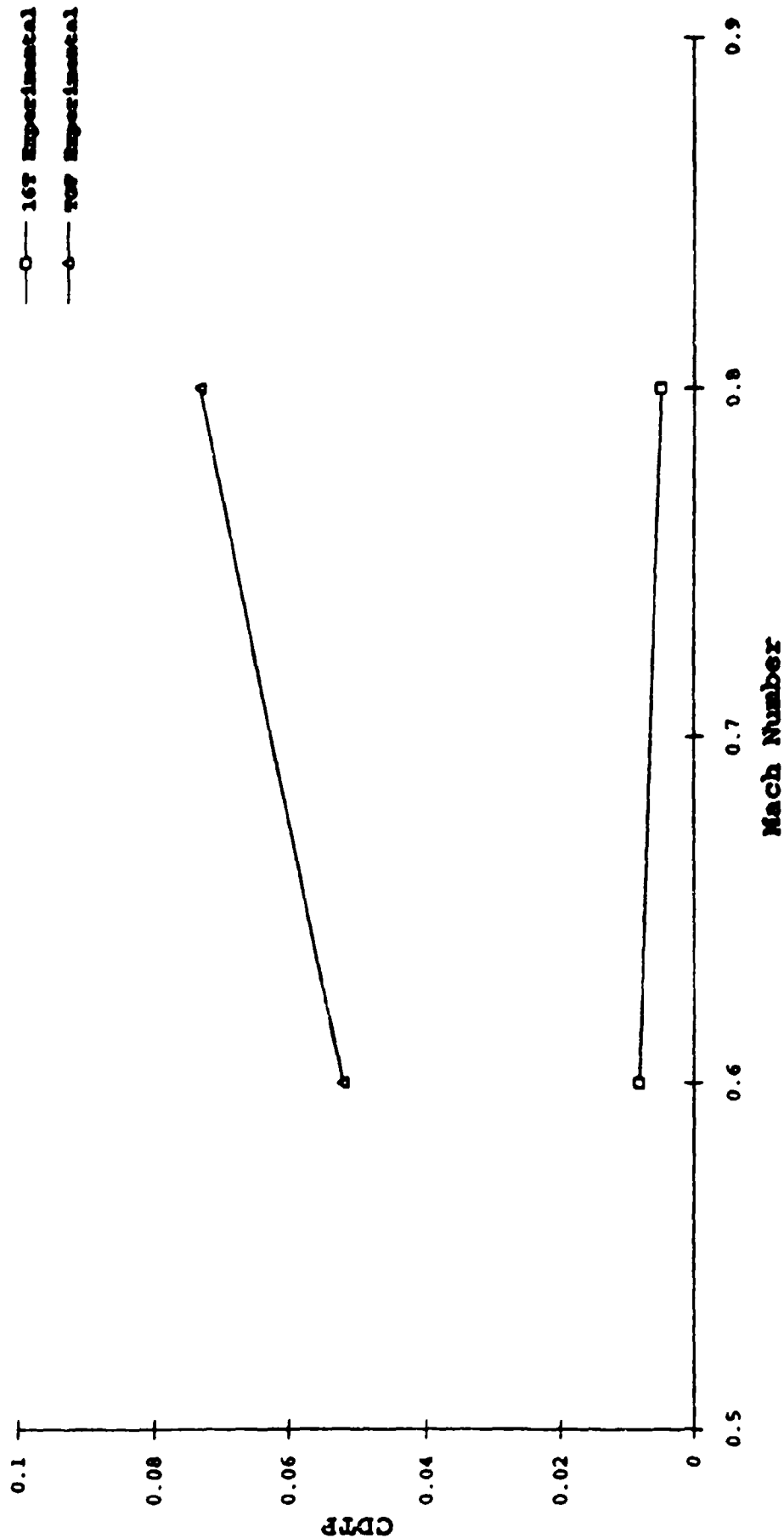
Figure 15(b). Comparison of Pressure Drag Coefficients Between Facilities
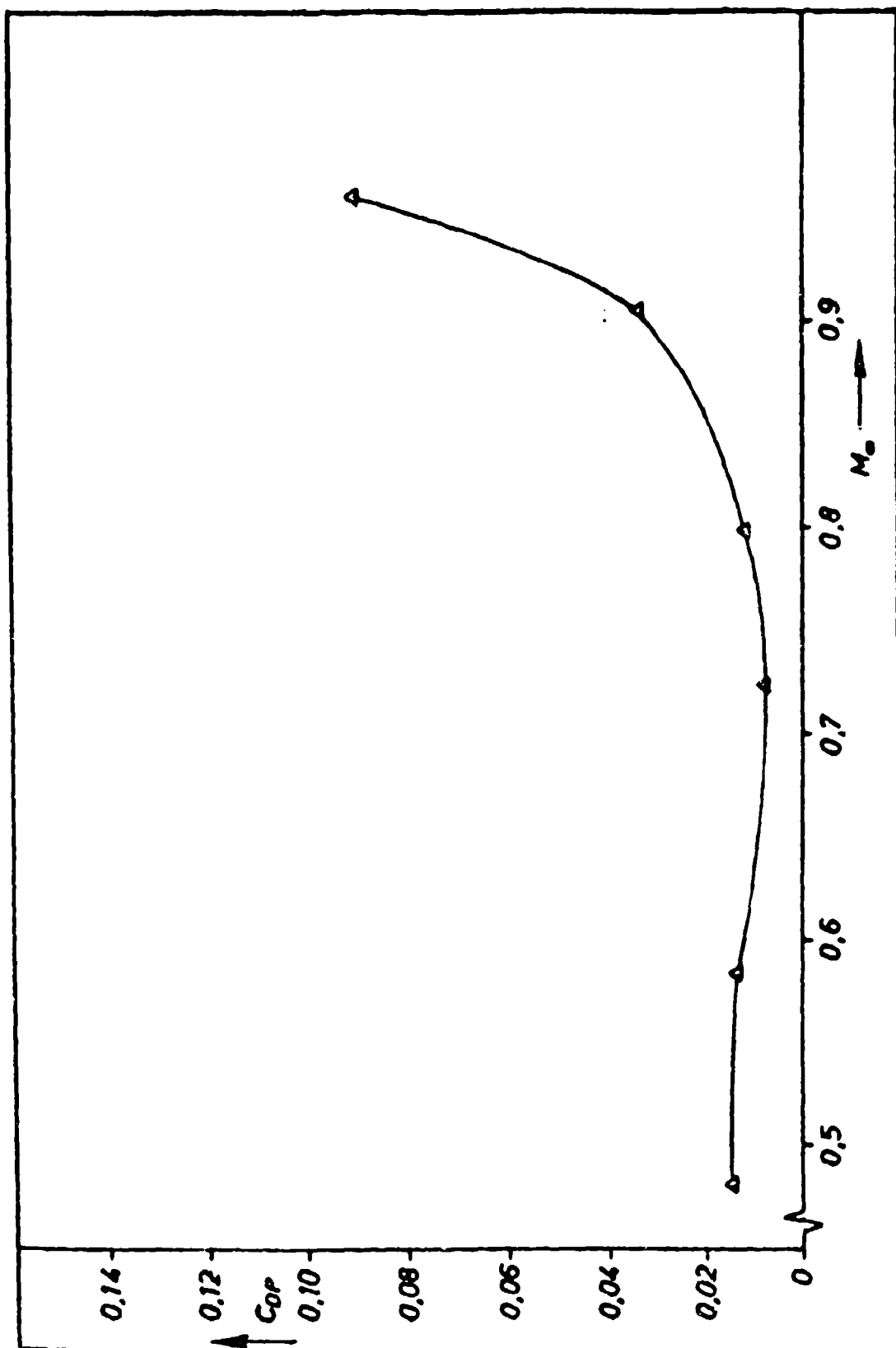
Figure 16. Typical Pressure Drag Coefficient vs. Mach Number Plot for Axisymmetric Boattail Configurations
(Reference 5)

10 Deg. Boattail, 16T Experimental Data
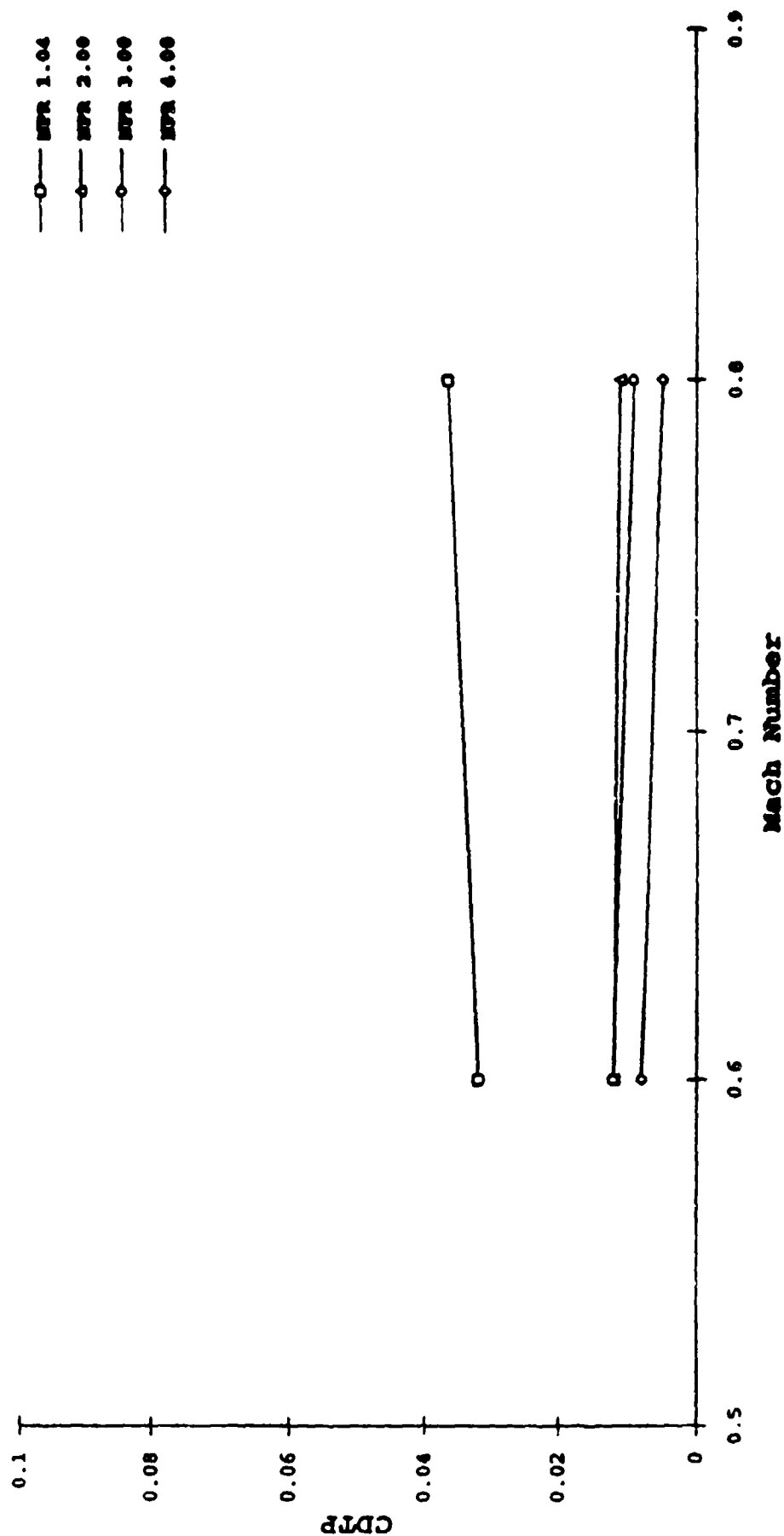
Figure 17(a). Comparison of Pressure Drag Coefficients Between NPRs Compared Incrementally Between Facilities

55

10 Deg. Boattail, TGF Experimental Data

NPR 1.04
NPR 2.00
NPR 3.00
NPR 4.00

CDTP

Mach Number

Figure 17(b). Comparison of Pressure Drag Coefficients Between NPRs Compared Incrementally Between Facilities

56

10 Deg. Boattail, Mach 0.6

Figure 18(a). Comparison of Pressure Drag v. NPR Between Facilities

57

15 Deg. Boattail, Mach 0.8

CDTP

NPR

— 1ST Experimental
— TOP Experimental

0.1 0.08 0.06 0.04 0.02 0

0 1 2 3 4 5

Figure 18(b). Comparison of Pressure Drag v. NPR Between Facilities
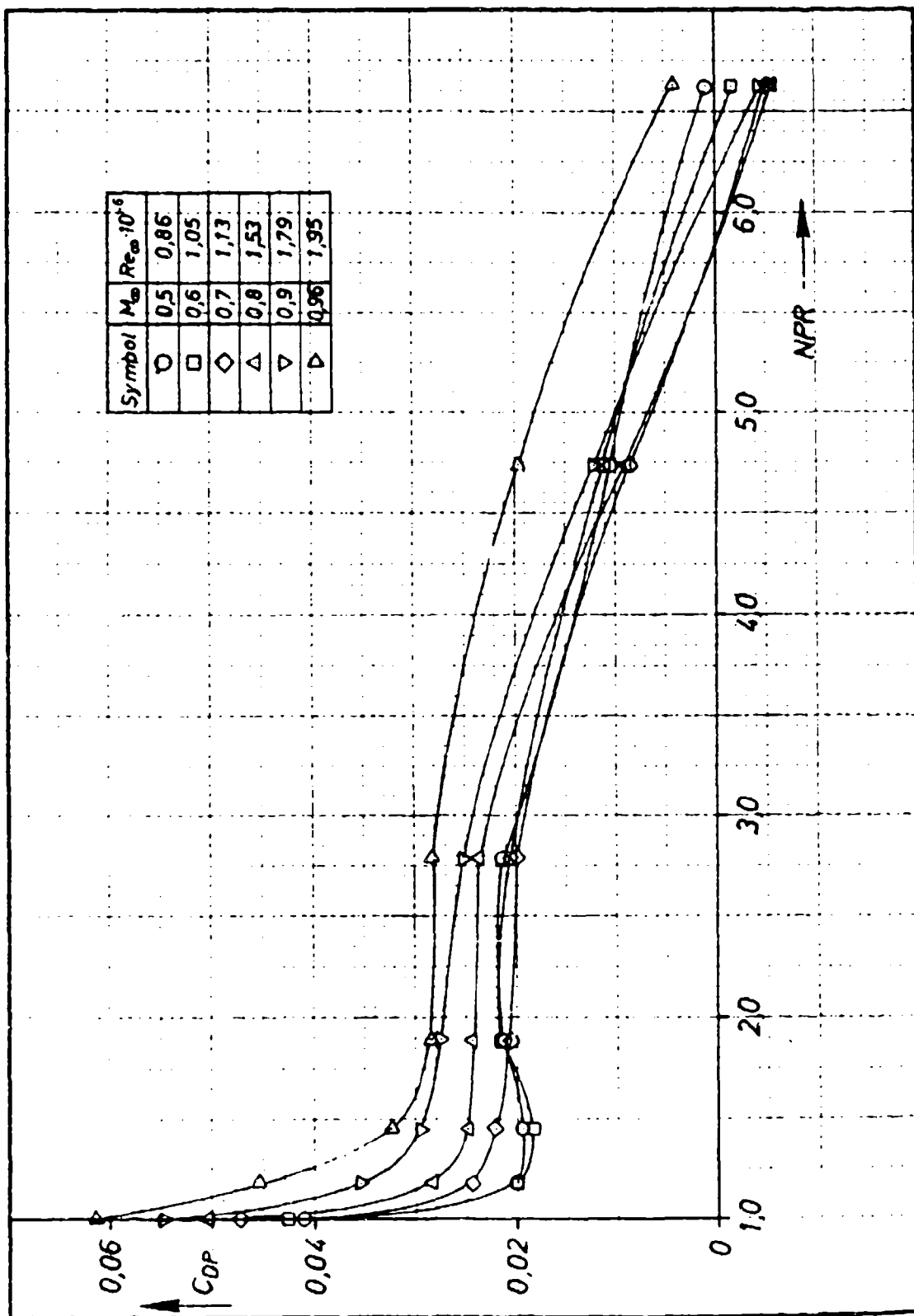
Figure 19. Typical Pressure Drag Coefficient vs. NPR Plot for Axisymmetric Boattail Configurations (Reference 5)
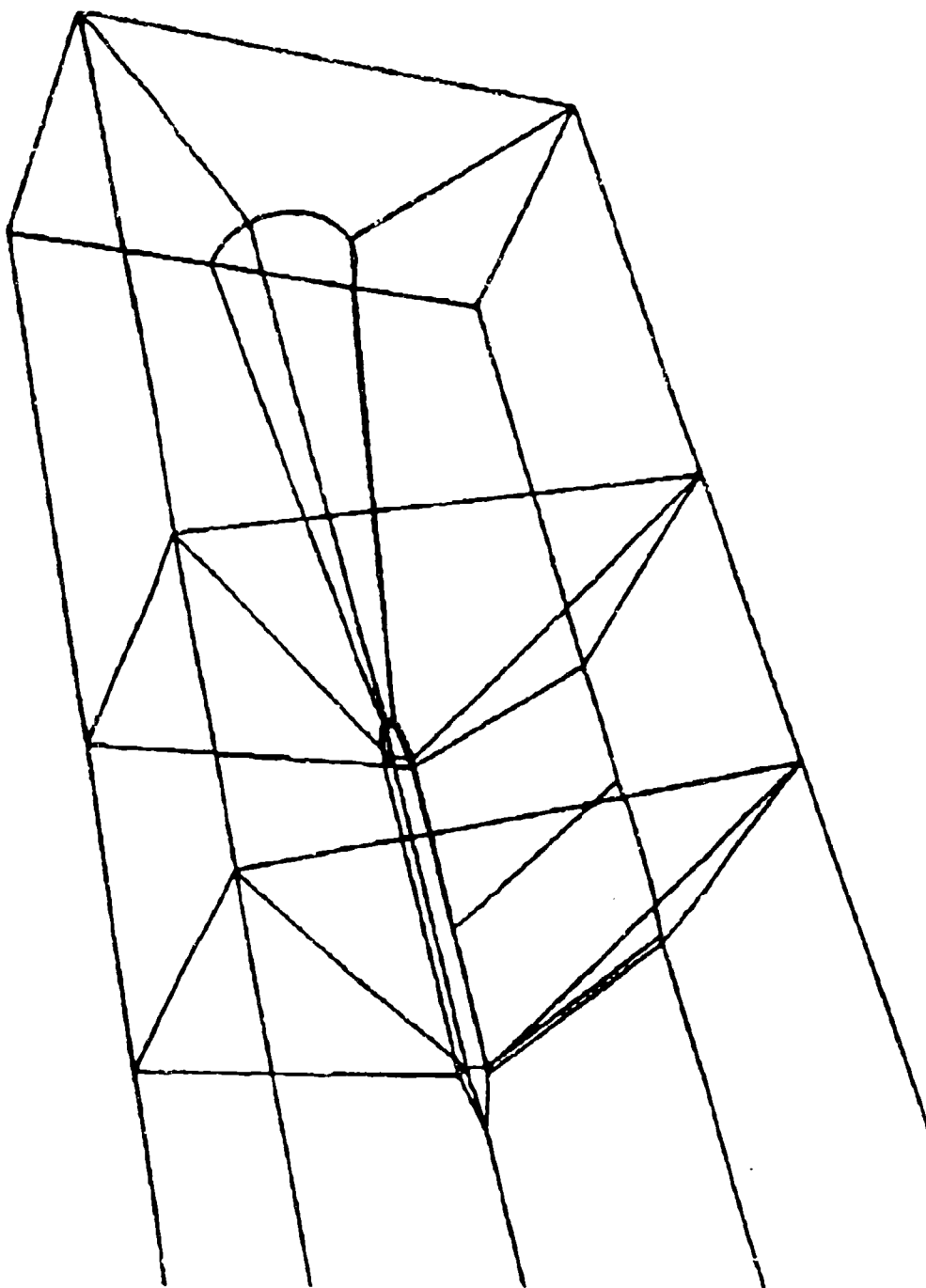
Figure 20(a). Blocking Strategies, TGF and 16T Test Sections

60

TGF Test Section Blocking Strategy, 3D View
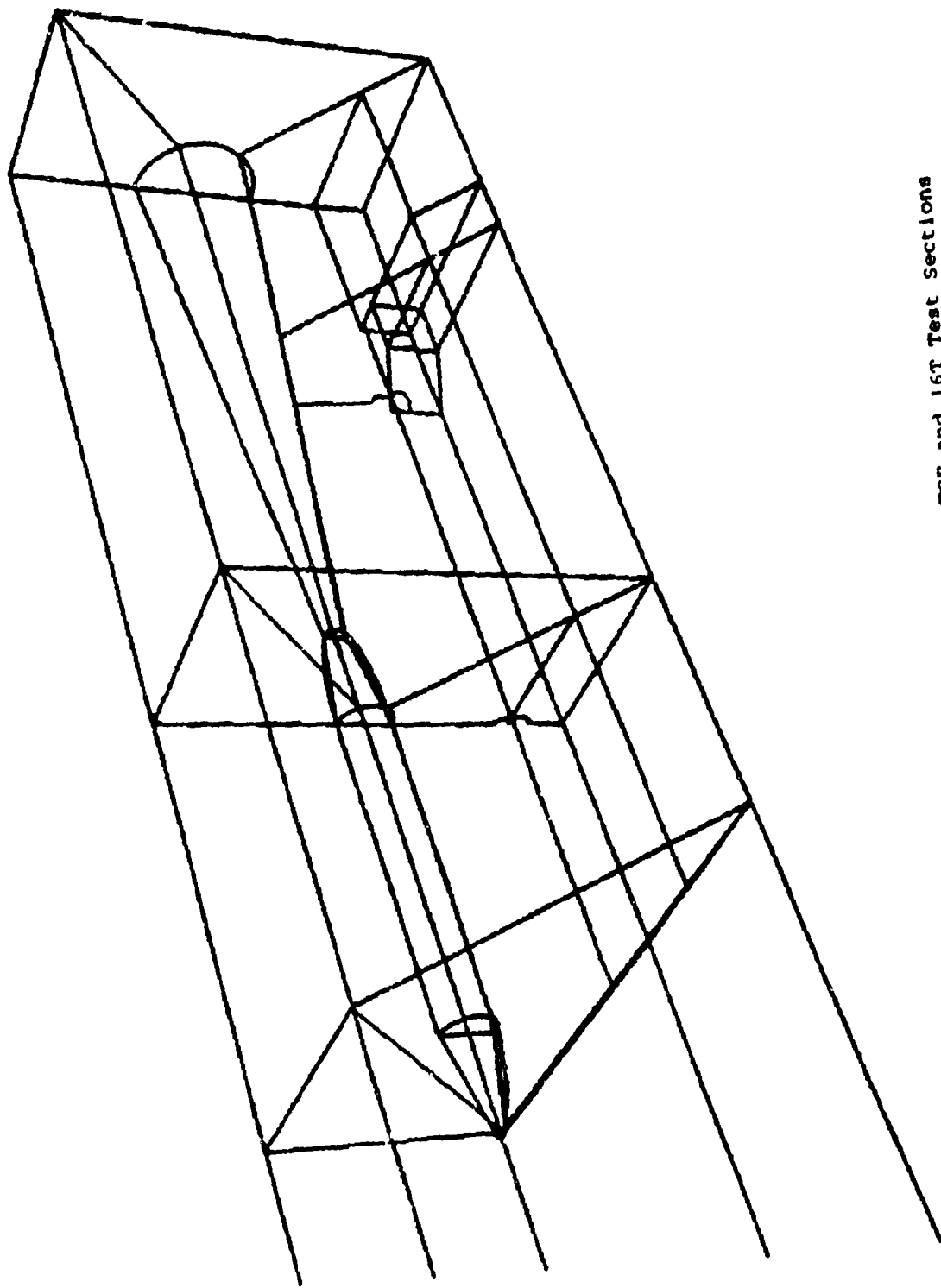
Figure 20(b). Blocking Strategies. TGF and 16T Test Sections

61

16T Test Section Grid Strategy, Cross-Sectional View
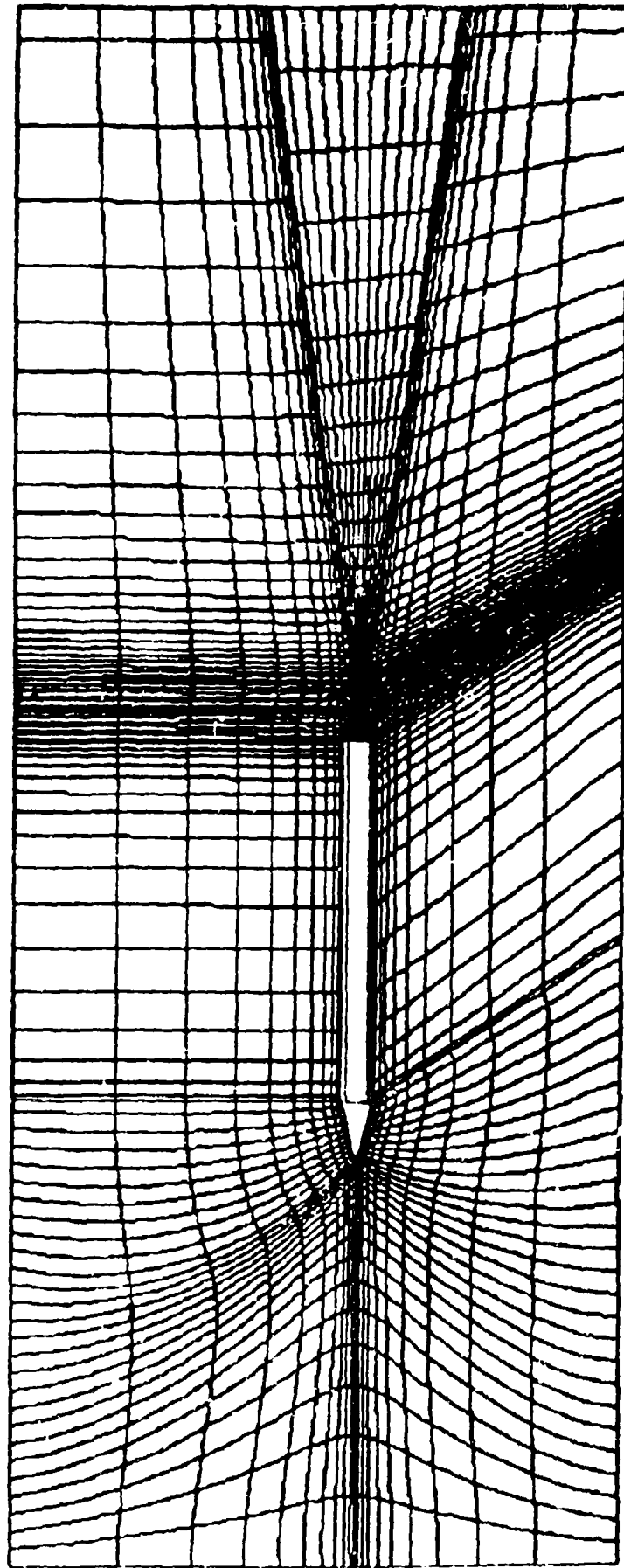
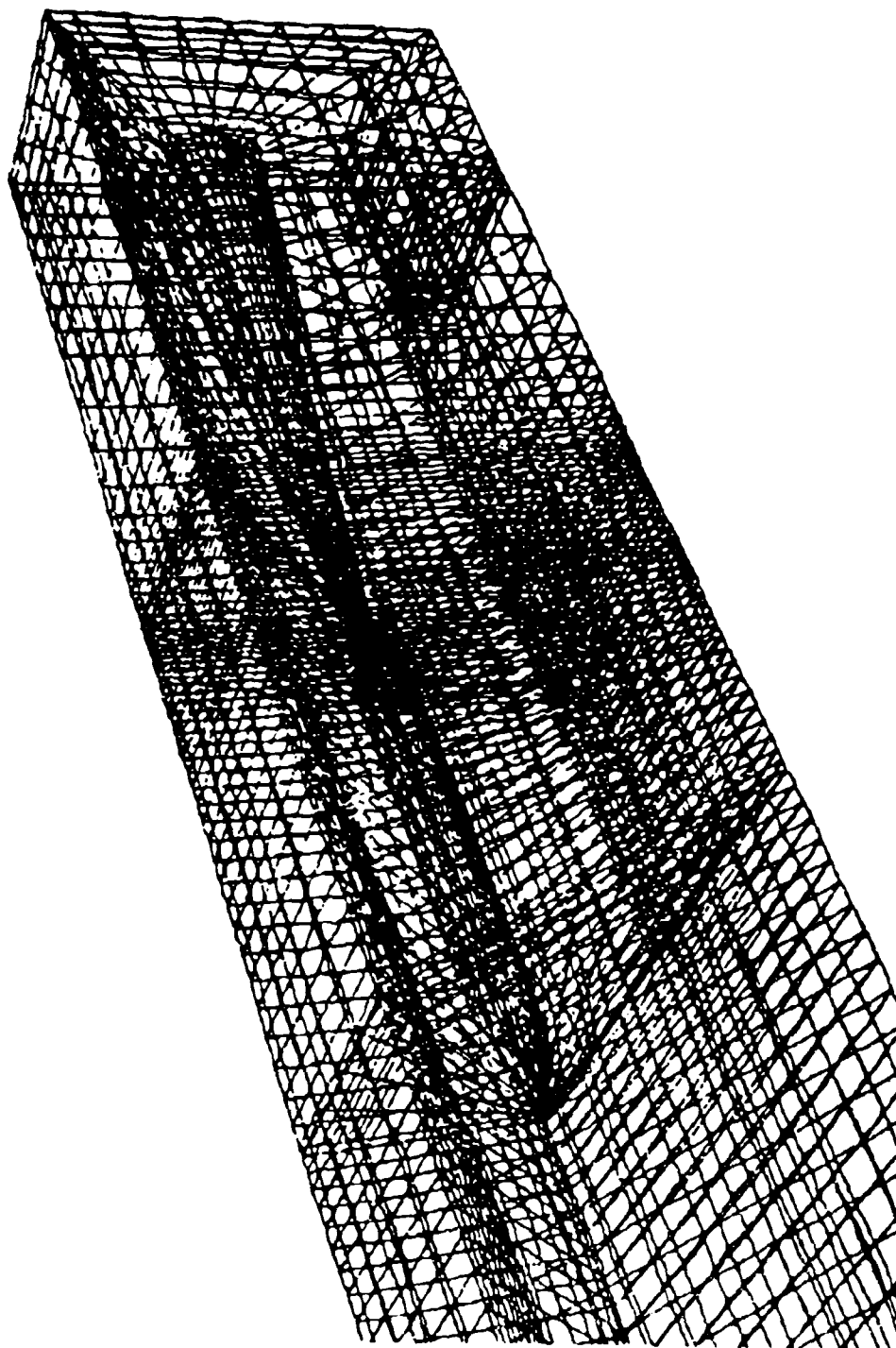Figure 21(o). Gridding Strategies. TGF and 16T Test Sections. 2D and 3D Views

TGF Test Section Grid Strategy, Cross-Sectional View
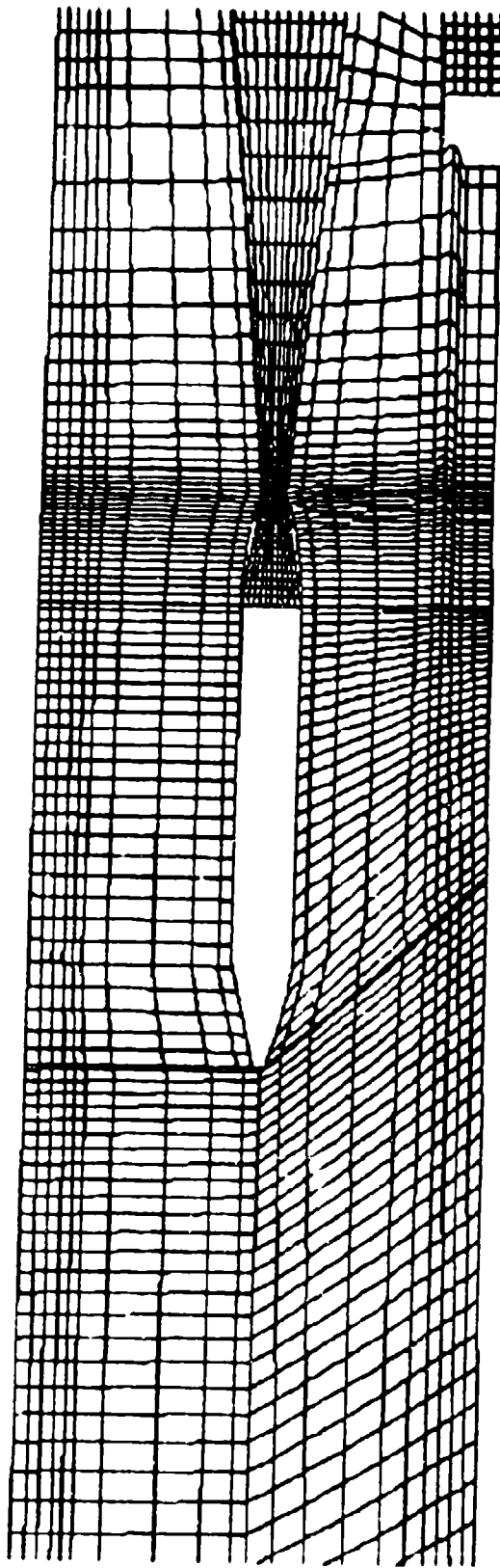
Figure 21(b). Gridding Strategies, TGF and 16T Test Sections, 2D and 3D Views

63

16T Test Section Grid Strategy, 3D View
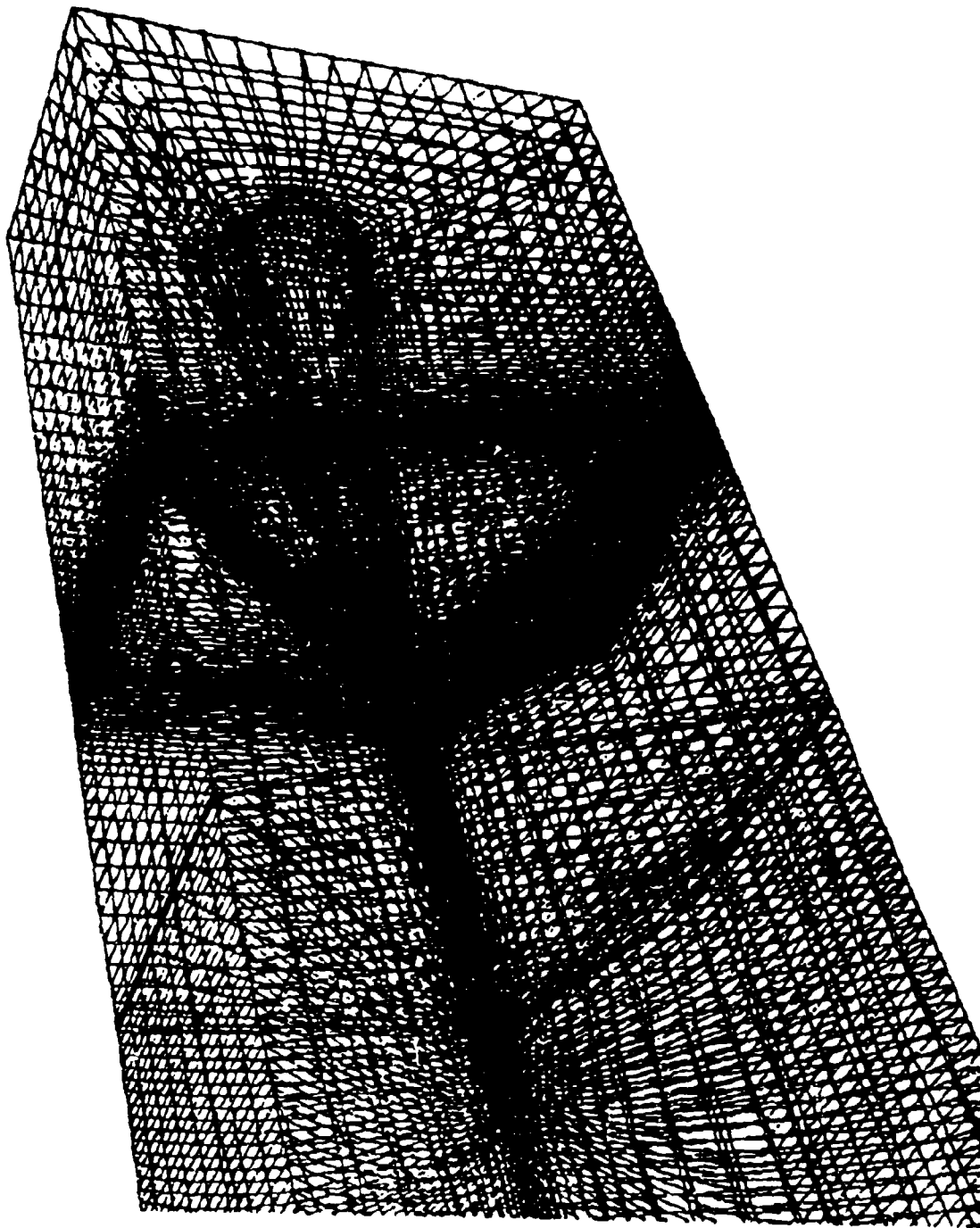
Figure 21(c). Gridding Strategies, TGF and 16T Test Sections. 2D and 3D Views

64

Figure 21(d). Gridding Strategies, TGF and 16T Test Sections, 2D and 3D Views

65

Facility/TPN	Mach Number	NPR	Boattail Angle
16T/6102	0.599	1.04	10 deg
16T/8609	0.601	3.01	10 deg
16T/6204	0.801	1.08	10 deg
16T/6211	0.799	3.14	10 deg
TGF/63	0.605	1.04	10 deg
TGF/66	0.606	3.01	10 deg
TGF/170	0.803	1.06	10 deg
TGF/224	0.804	3.02	10 deg

Figure 22. TGF Validation Study CFD Test Matrix

Figure 23. The 16T CFD Results, Mach 0.6, NPR 1.04, Centerline Cp Contours

67

10 Deg. Boattail, Mach 0.6, NPR 1.04

o   16T Experimental

..... 16T CFD

Cp

Model Station (scaled to TOP stations in inches)

Figure 24. 16T CFD Results Compared With Experimental, Mach 0.6, NPR 1.04, Centerline Cp Distribution
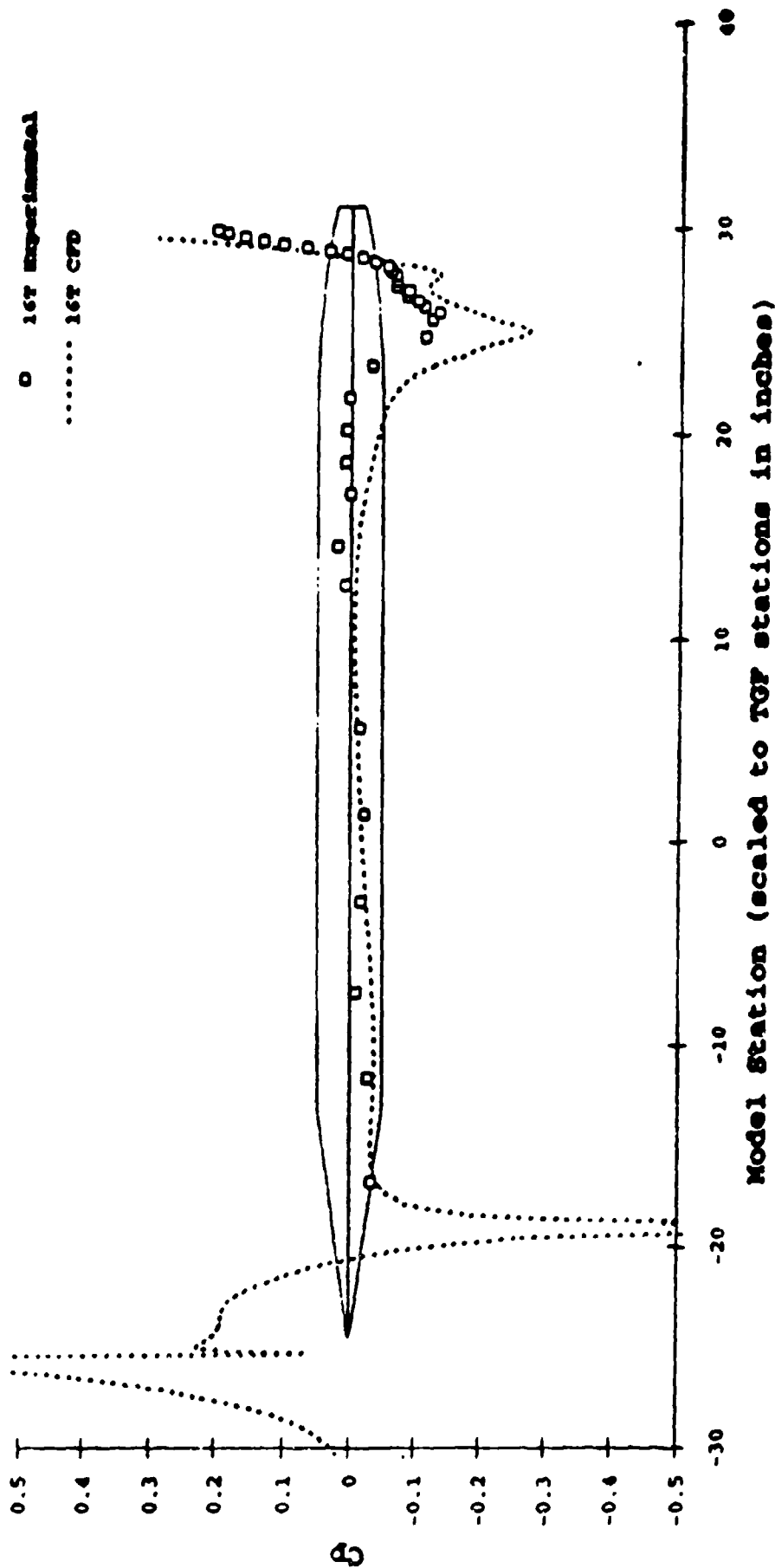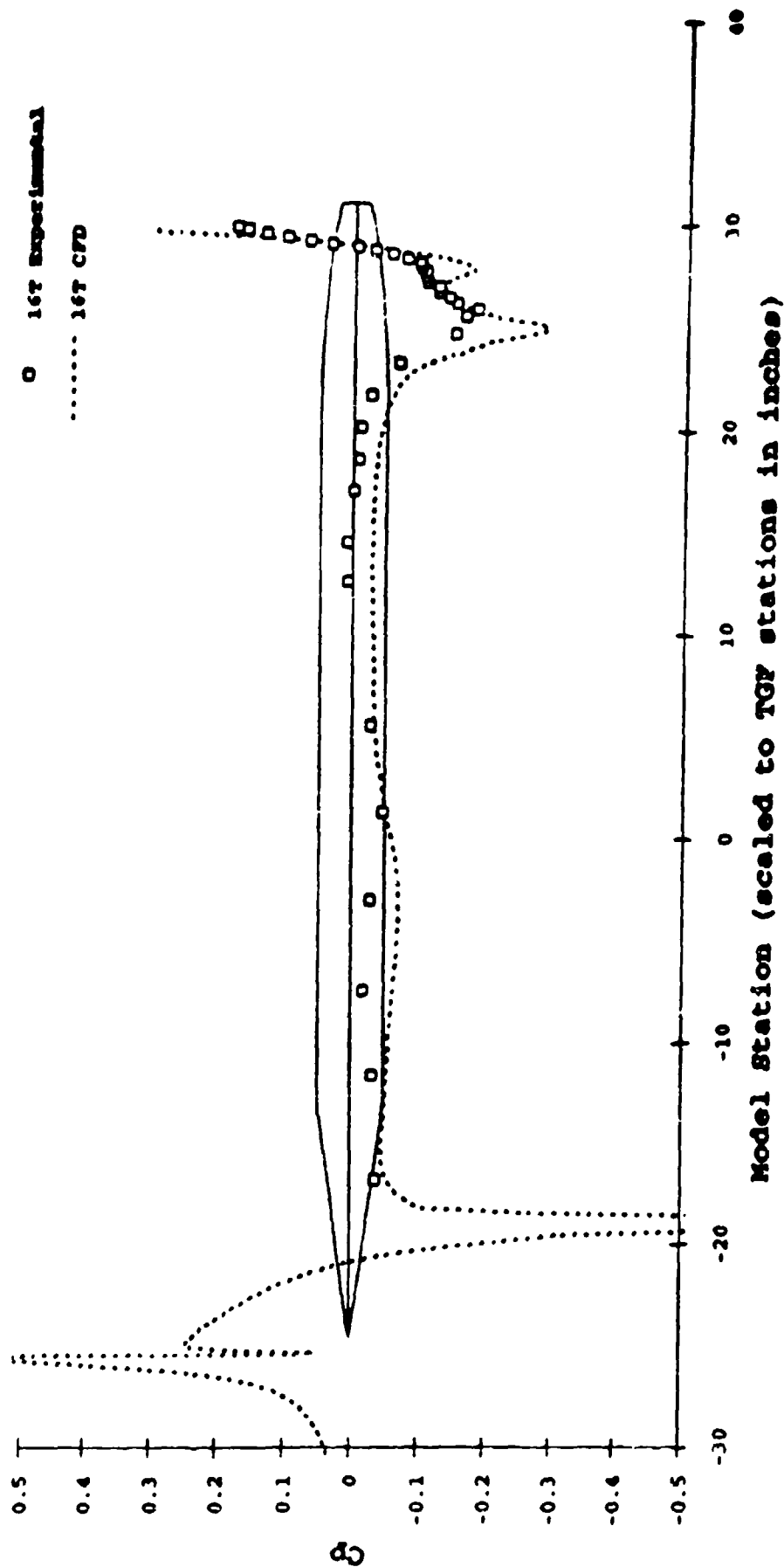
68

10 Deg. Boattail, Mach 0.6, NPR 3.00

Figure 25. 16T CFD Results Compared With Experimental, Mach 0.6, NPR 3.00, Centerline Cp Distribution

69

10 Deg. Boattail, Mach 0.8, NPR 1.04

Figure 26. 16T CFD Results Compared With Experimental. Mach 0.8, NPR 1.04, Centerline Cp Distribution
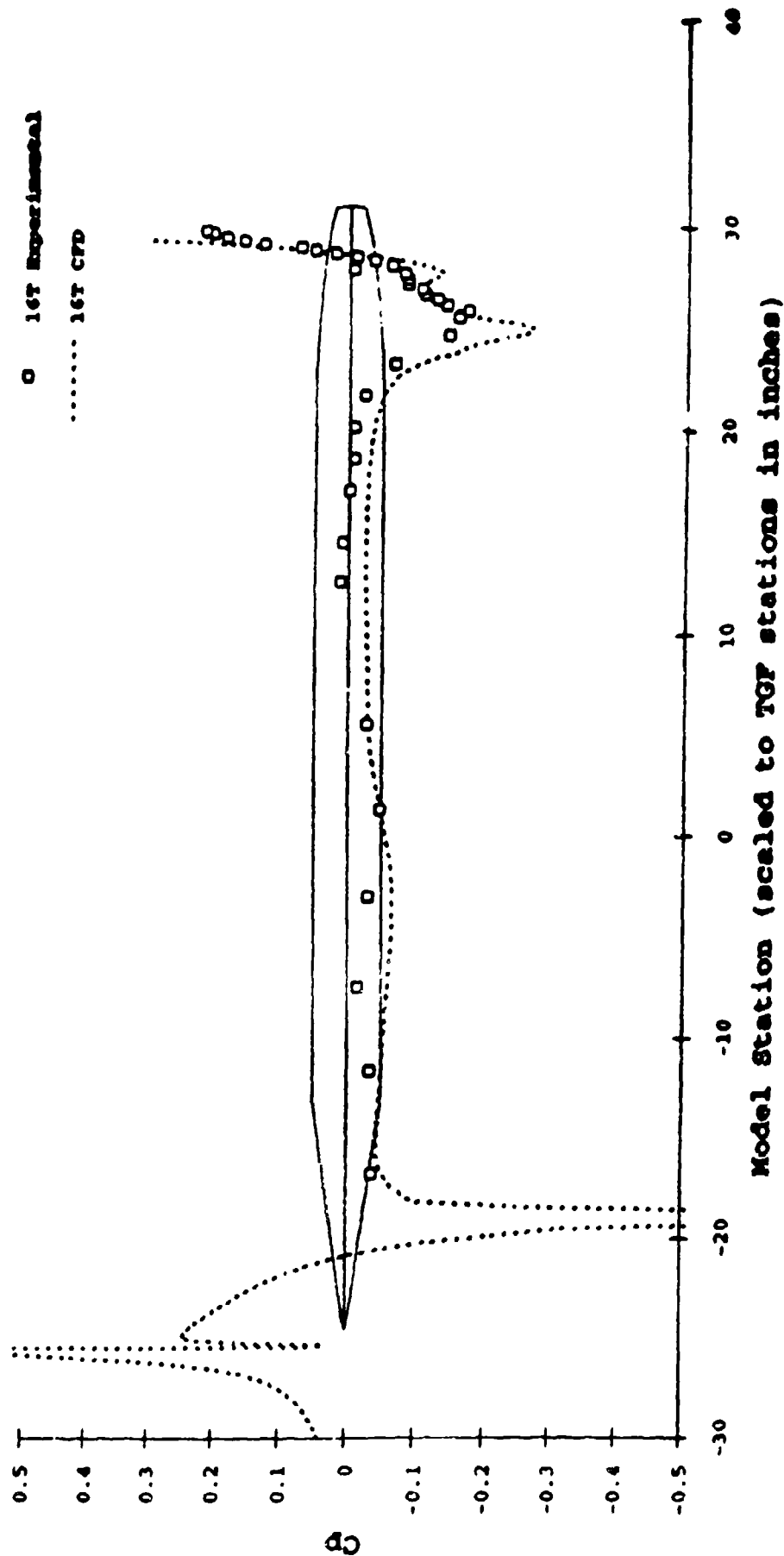
10 Deg. Boattail, Mach 0.8, NPR 3.00

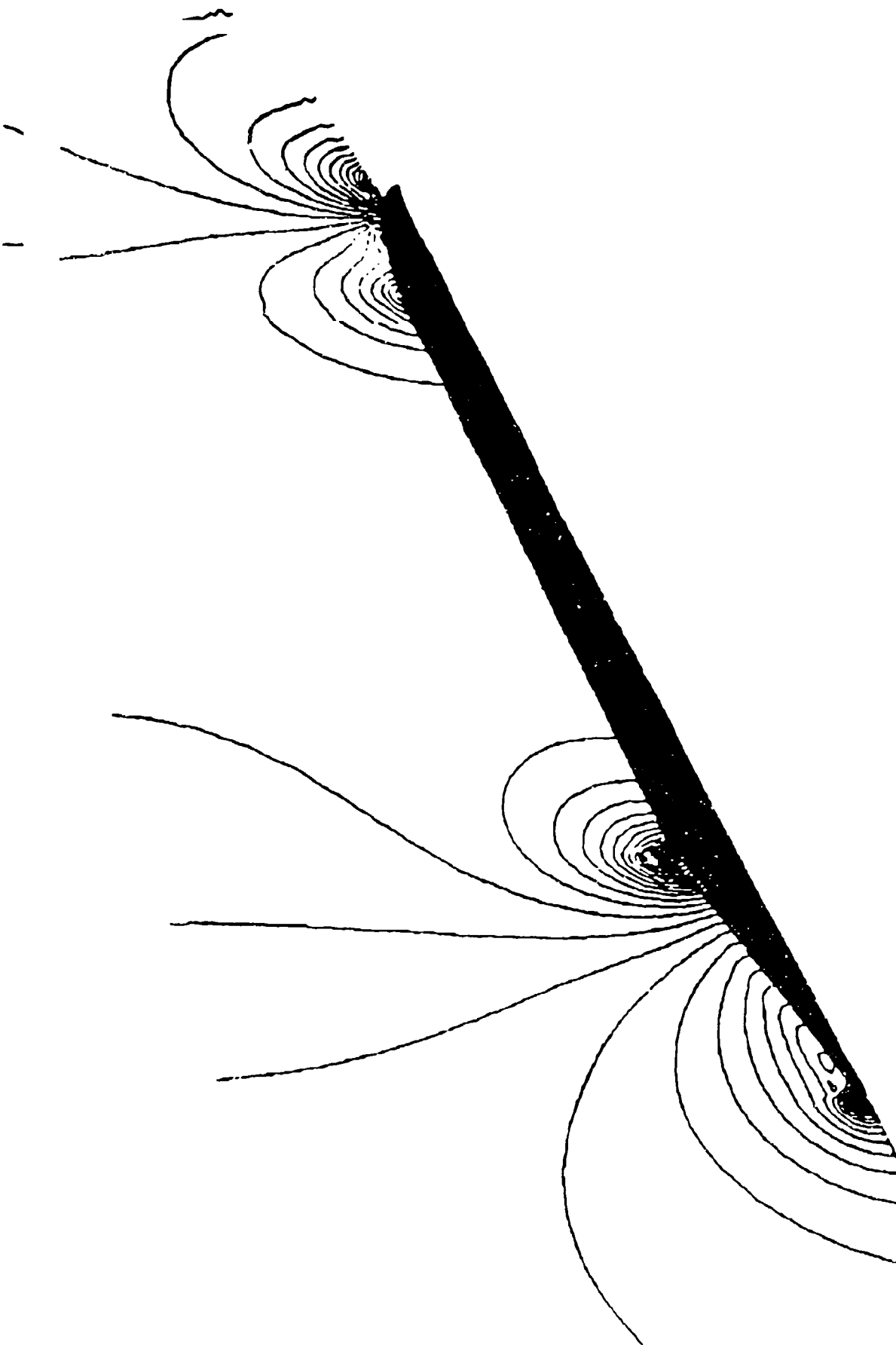Figure 27. 16T CFD Results Compared With Experimental. Mach 0.8, NPR 3.00. Centerline Cp Distribution

71

Figure 28. TCF CFD Results, Mach 0.6, NFR 1.04, Centerline Cp Contours
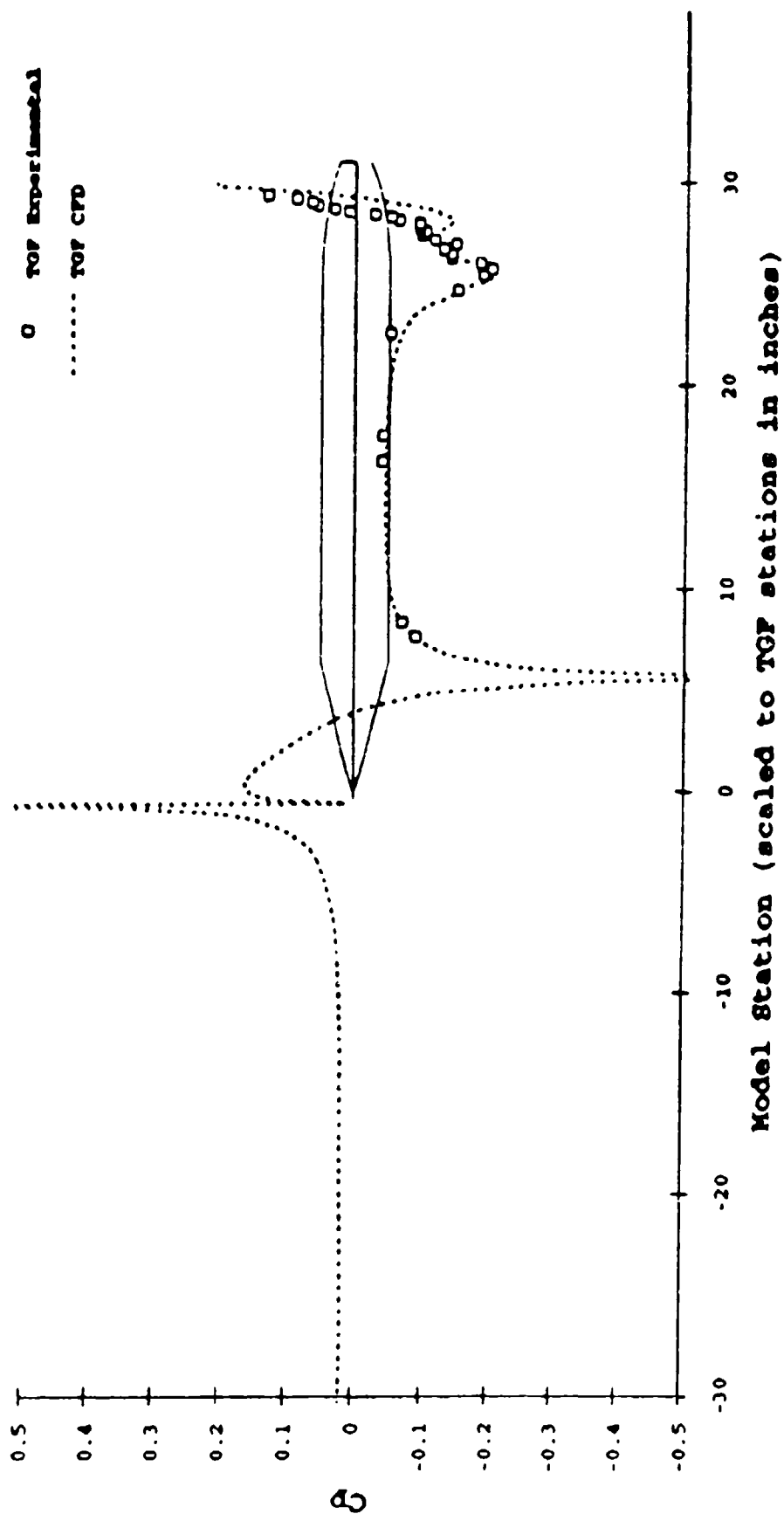
10 Deg. Boattail, Mach 0.6, NPR 1.04

Figure 29. TGF CFD Results Compared with Experimental, Mach 0.6, NPR 1.04, Centerline Cp Distribution
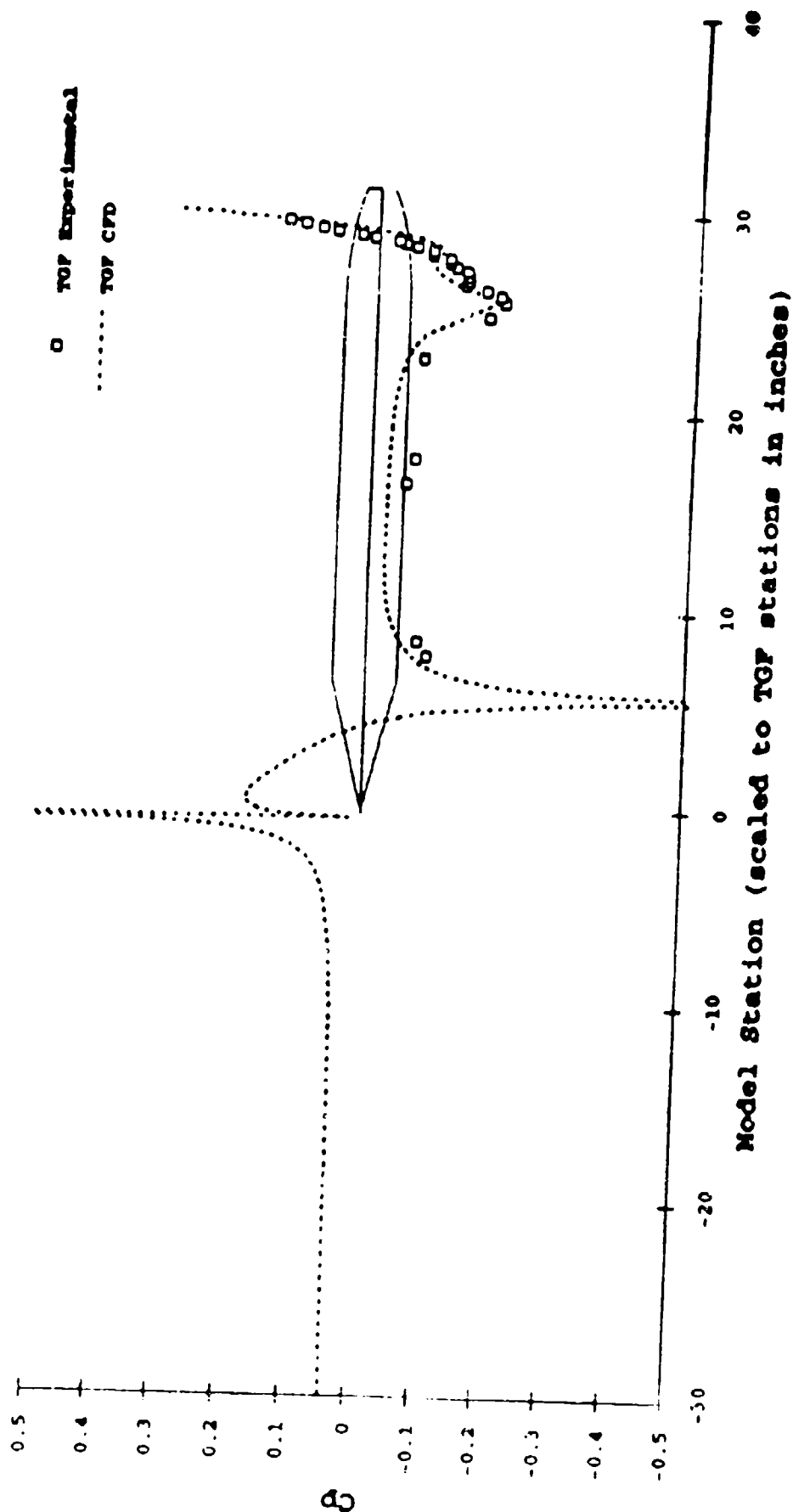
10 Deg. Boattail, Mach 0.6, NPR 3.00

Figure 30. TGF CFD Results Compared With Experimental, Mach 0.6, NPR 3.00, Centerline Cp Distribution

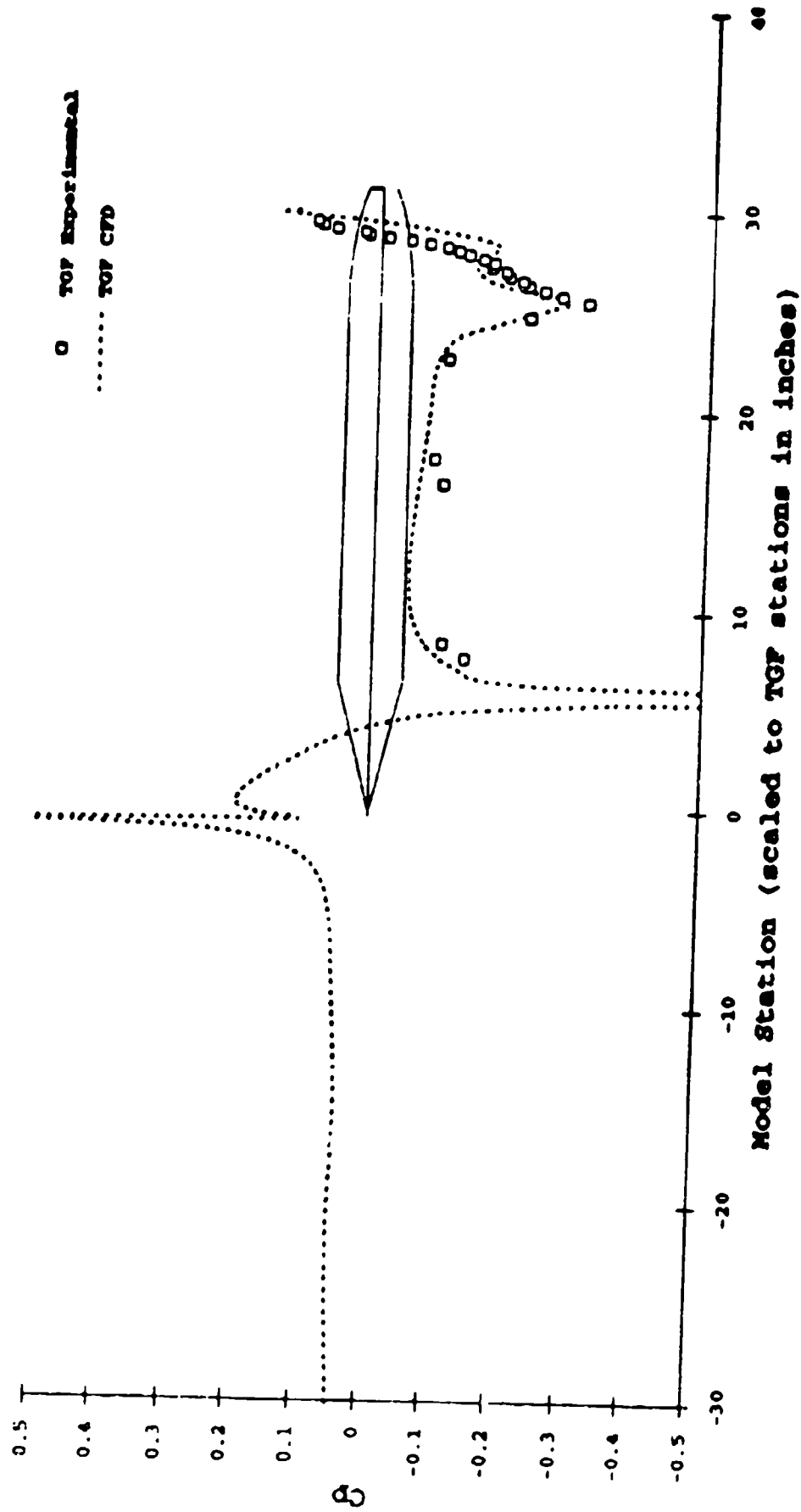# 10 Deg. Boattail, Mach 0.8, NFR 1.04

o TGP Experimental

.... TGP CFD

Model Station (scaled to TGP stations in inches)

Cp

Figure 31. TGP CFD Results Compared With Experimental, Mach 0.8, NPR 1.04, Centerline Cp Distribution
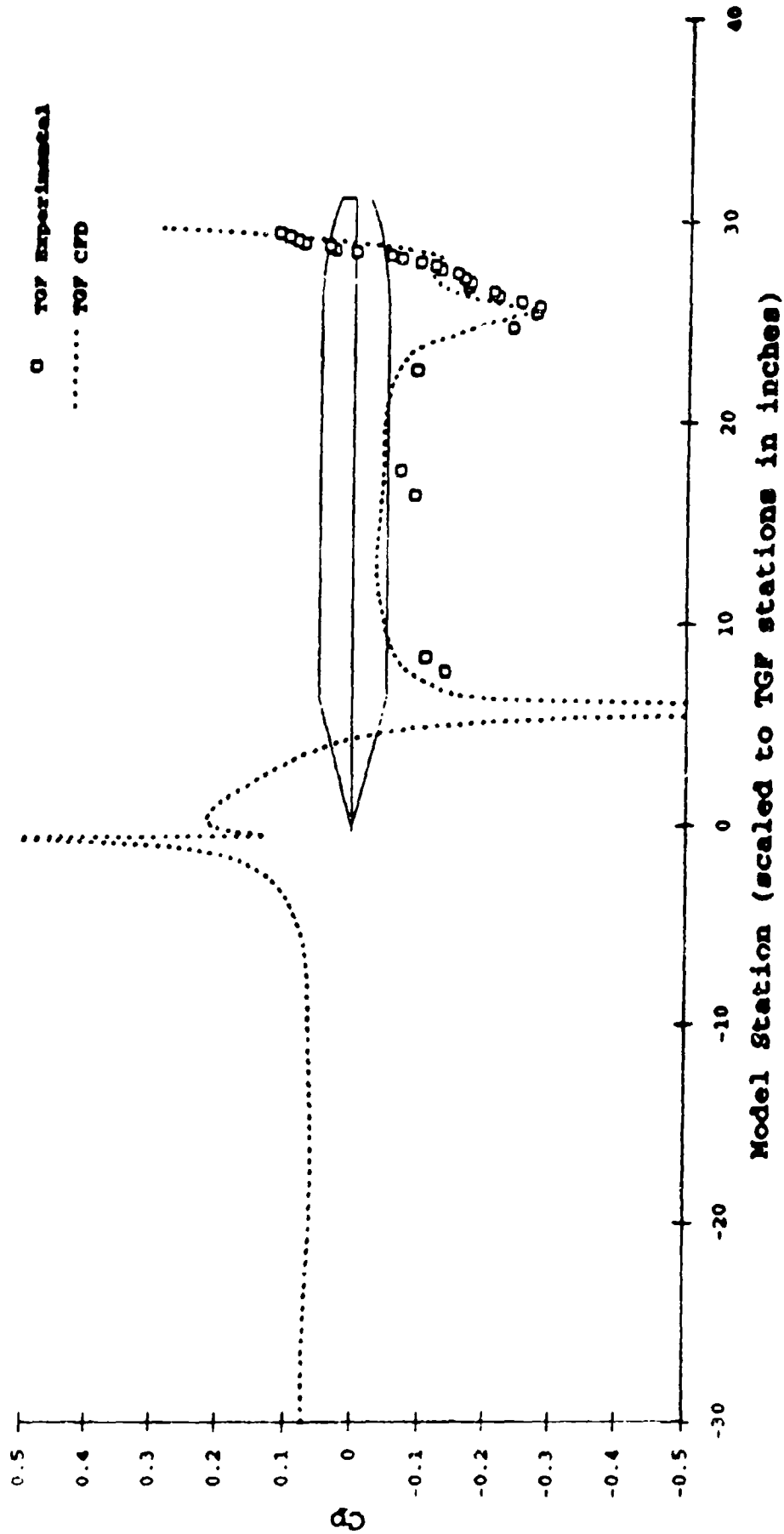
75

10 Deg. Boattail, Mach 0.8, NPR 3.00

Figure 32. TGF CFD Results Compared With Experimental, Mach 0.8, NPR 3.00, Centerline Cp Distribution

10 Deg. Boattail, Mach 0.6, NPR 3.00

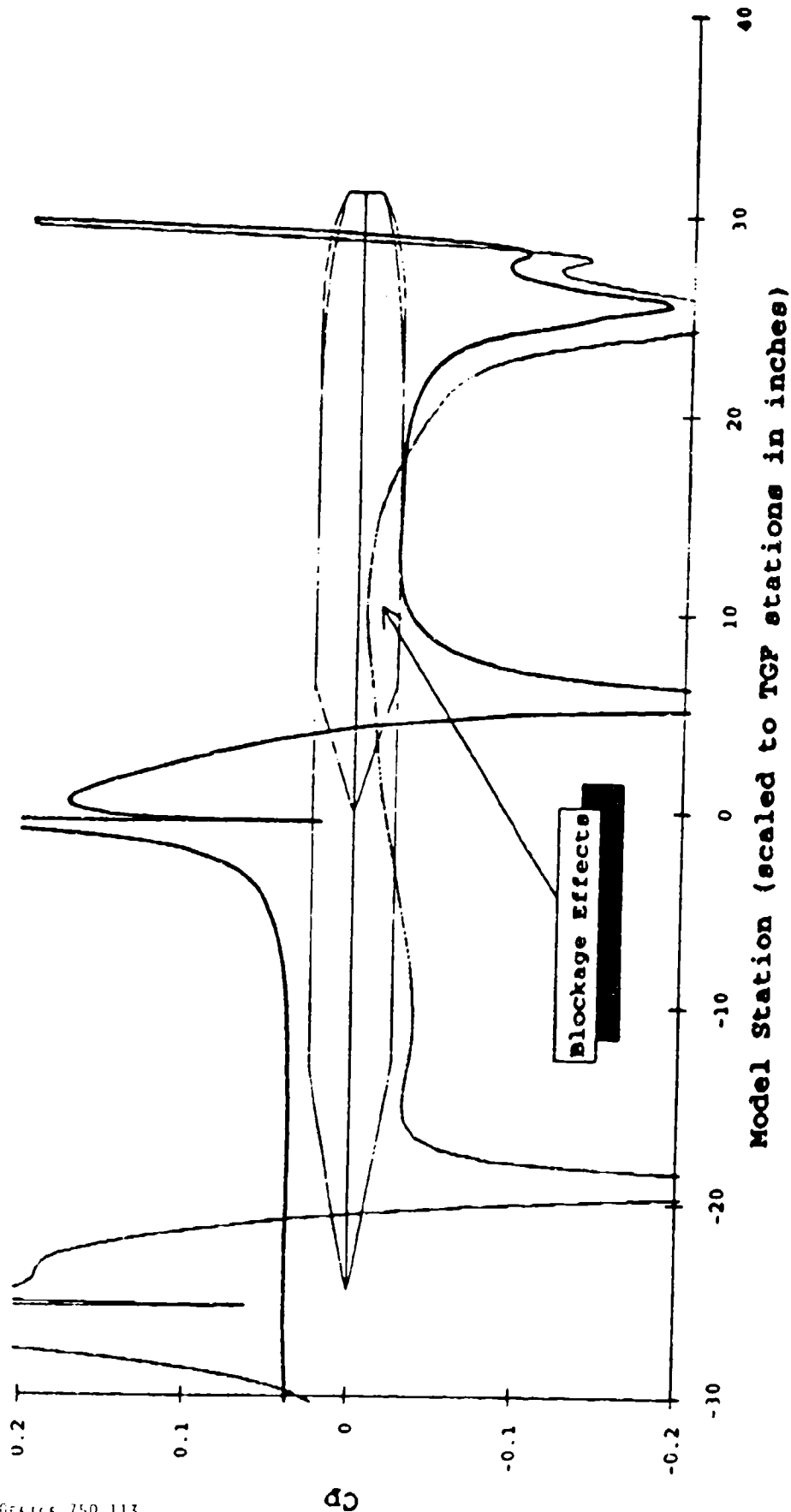Figure 33. CFD Comparison Between Facilities Showing Effect of Blockage

END

FILMED

DATE: 7-93

DTIC